Eur. Phys. J. D (2020) 74: 90
https://doi.org/10.1140/epjd/e2020-100646-0

THE EUROPEAN PHYSICAL JOURNAL D

Topical Review

Recent total cross section measurements in electron scattering from molecules

Czesław Szmytkowski[a] and Paweł Możejko[b]

Department of Atomic, Molecular and Optical Physics, Faculty of Applied Physics and Mathematics, Gdańsk University of Technology, ul. Gabriela Narutowicza 11/12, 80-233 Gdańsk, Poland

Received 23 December 2019 / Received in final form 9 March 2020
Published online 5 May 2020

Abstract. The *grand*-total cross sections (TCSs) for electron scattering from a range of molecules, measured over the period 2009–2019 in various laboratories, with the use of different electron transmission systems, are reviewed. Where necessary, the presented TCS data are also compared to earlier results. Collection of investigated molecular targets (biomolecules, biofuels, molecules of technological application, hydrocarbons) reflects their current interest in biology, medicine, ecology and industry. Most of measurements covered the energy range from about 1 eV to some hundreds of eV, with a few exceptions extending those limits down to near thermal or up to almost high impact energies. The importance of reliable TCS data in the field of electron-scattering physics is emphasized. Problems encountered in TCS experiments are also specified.

1 Introduction

Over 120 years after electron discovery by Thomson [1], more than 110 years after the first electron collision experiments of Lenard [2] and Franck-Hertz [3], almost 100 years from pioneering electron scattering experiments performed by Ramsauer [4] and over 45 years after identification of electron resonances in electron-atom and electron-molecule collisions by Schulz [5], accurate new experimental data on electron interactions with matter are still crucial and desired for understanding a wide variety of natural and technological processes occurring and carried on in complex environments. One of the examples is Rosetta mission in which glycine molecules have been discovered in the coma of the comet 67P/Churymov-Gerasimenko [6]. Measured with ROSINA (Rosetta Orbiter Spectrometer for Ion and Neutral Analysis) mass spectrometer relative abundances of glycine have been evaluated using theoretical electron-impact ionization cross section while sensitivity of mass spectrometer has been tested using electron scattering cross section data for noble gases [6,7]. The important role of low energy electrons (LEEs) in such extreme astrochemical and astrobiological environments has also been demonstrated in many experiments performed in laboratories [8,9]. It has been shown that irradiation of ammonia and acetic acid mixture condensed at 25 K by LEEs leads to a chemical reaction in which glycine is created [10]. Recently, the formation of that simple amino acid building block of proteins has been also observed in CO_2:CH_4:NH_3 ices irradiated by 0–70 eV electrons in mass selected temperature programmed desorption [11]. For the interpretation of experiments carried out in complex condensed environment the electron scattering data at the molecular level are very helpful [12].

The knowledge of the efficiency of electron interactions with biomolecules is very crucial for description and modeling of ionizing radiation damage to living cells and biomolecules radiolysis. After the discovery that the secondary electrons of low energy can be involved in DNA double and single strand brakes [13–15] the complete data sets of reliable cross sections for electron scattering from biomolecular subunits and analogs are needed and continuously updated [16–18]. Such data are also necessary for the ionizing radiation modeling via Monte Carlo simulations [19,20]. Unfortunately, the required collisional data are limited as yet [17,21]. What more, significant discrepancies between available experimental results still exist, even for quite simple molecular targets like water molecule [22–24].

Accurate experimental data concerning electron interactions are also important for the description of many phenomena occurring in plasma physics and gaseous electronics [25,26], including modeling of processes in cometary and planetary atmospheres [27–29]; they are also of great importance for modern technologies including focused electron beam induced deposition (FEBID) [30,31]. More

[a] e-mail: czsz@mif.pg.gda.pl
[b] e-mail: paw@pg.edu.pl

details on the present status of electron collision physics including preview of electron collisions theory, electron-molecule interactions, ionization and dissociative electron attachment studies with the summary of the future challenges can be found in one of the road maps on photonic, electronic and atomic collision physics [32].

Since almost the first data collections from pioneering investigations on electron scattering phenomena [33,34] a lot of review papers on experimental and theoretical studies devoted to electron collisions with atoms and molecules have been published [35–46], just quote a few representative.

The aim of this paper is to review the *grand*-total cross section (TCS) energy dependences for electron scattering from molecular targets obtained by various experimental groups during the period 2009–2019. Where necessary, earlier TCS data are also included to compare with the new results. The described TCS data sets cover the interval of electron impact energy from 0.04 eV to 4500 eV. TCS values are presented in 10^{-20} m^2 units.

For the purpose of this review, only some remarks on the *grand*-total electron-scattering cross section quantity and the arguments for its measuring are given. The idea of electron-transmission method, mostly used in absolute TCS experiments, is then shortly presented; main factors which can influence the accuracy of the measured TCSs are specified and discussed. Description of experimental techniques used for the TCS determination in various laboratories (listed in Tab. 1) is not the purpose of the present work. Details on the principles and techniques of the transmission method can be found in comprehensive papers written by Bederson and Kieffer [35], Kennerly and Bonham [47], Trajmar and Register [48], Ma et al. [49] and Brunger [50] and/or in the original papers cited in Table 1.

Theoretical studies on the electron–molecule scattering are not presented and discussed here. Comprehensive reviews with data compilations and description of theoretical methods and computational procedures, which can be utilized in cross section calculations (including TCS computations), can be found elsewhere (e.g. [38,51–53] and references therein).

The review and tables of experimental cross sections for electron scattering from atoms and molecules, including total cross sections collected up to 2011, have been presented by Raju [54]. Electron-molecule total cross section collection up to the beginning of the XXI century can be found also in [55].

2 Grand-total cross-section, TCS

The *grand*-total cross section (TCS) for projectile scattering from a target is the sum of the integral cross sections (ICSs) for all projectile–target interaction processes accessible at a given impact energy. Due to its summary nature, the TCS is only a measure of the probability that projectile–target interaction of any type occurs, without information on the contribution of specific scattering events.

The exemplary contribution of integral cross sections for particular collisional processes to the *grand*-total cross section is illustrated in Figure 1 (log–log) in which the recommended *grand*-total cross section for electron collisions with CF_4 molecule is depicted together with recommended or suggested cross sections for particular scattering channels like elastic scattering, electron-impact dissociation and ionization, electron attachment, and vibrational excitation [45].

The subtle structures visible in the energy dependence of cross sections for particular scattering channels are in the TCS energy function apparently smoothed out or even imperceptible. Therefore, to explain TCS variation with impact energy, especially the origin of its spectacular features, complementary results concerning various scattering processes are indispensable. On the other hand, the appearance of any features in the TCS energy curve indicates the energy region which may be worth of further, more detailed investigations.

Nevertheless, in spite of a low position in the ranking of different cross sections, the TCS data alone also give valuable information on the scattering phenomena. An advantage of TCS over the variety of measurables describing the scattering process is the fact that TCS can be measured in absolute scale over wide energy range; all quantities necessary to determine the TCS can be measured or directly estimated in experiment and therefore TCS values can be obtained without any normalization procedure.

Furthermore, among cross sections, the TCS is considered to be one of the most accurate; declared overall experimental uncertainties of reported TCS data are usually lower than 10%. That is why the experimental TCS may serve as one of the ranges of experimental quantitative tests of the reliability of theoretical models and computational procedures. As the sum of all integral cross sections, TCS represents the upper limit for any partial scattering cross section and therefore can be employed to check the consistency of compiled data sets. Reliable absolute TCS data may be used for rough but reasonable estimations of partial cross sections for targets for which such data are not available due to experimental and/or computational difficulties. They may be also utilized for the normalization of scattering intensities obtained in arbitrary units. Moreover, due to its accuracy, the TCS can be helpful in comparative studies. Comparison of TCS magnitudes and energy dependences for selected sequences of targets can reveal some regularities in the TCS behavior when going across the target series and give an insight into the role of molecular characteristics in the scattering dynamics. Any established TCS correlations with target parameters (e.g. the number of target electrons, an electric polarizability, a permanent electric dipole moment, the target structure and/or its geometry) can be utilized for the derivation of relevant semi-empirical formula, which in turn can be used in the cross section estimation for those targets for which electron-scattering data are still lacking.

Table 1 lists the laboratories in which the electron-scattering *grand*-total cross sections for molecular targets have been measured during the period of years from 2009 to 2019. Table specifies also targets which were investigated in these laboratories.

Table 1. Laboratories active in TCS measurements during the period 2009–2019 (in alphabetical order).

Laboratory	Molecular targets, and references in the text
Baylor University, Waco, USA	C_2H_4 (ethylene), C_3H_6 (propene), C_4H_8 (butene), C_4H_6 (1,3-butadiene) [144]; C_2H_2 (acetylene), C_3H_4 (propyne) [145]
Gdańsk University of Technology, Gdańsk, Poland	HCOOH (formic acid) [86]; C_4H_4O (furan) [87]; C_3H_3NO (isoxazole) [90]; C_5H_5N (pyridine) [107]; $C_5H_{10}O$ (tetrahydropyran) [111]; $(CH_3)_2CO$ (acetaldehyde) [116]; $(CF_3)_2CO$ (hexafluoroacetone) [117]; $X(CH_3)_4$ (X=C,Si,Ge) [126]; $SnCl_4$ [127]; C_4H_8 (1-butene, 2-methylpropene) [136]; C_5H_{10} (1-pentene) [138]; C_5H_{10} (2-methyl–2-butene), C_6H_{12} (2,3-dimethyl–2-butene) [137]; C_2H_2 (acetylene), C_4H_6 (1-butyne) [139]; C_4H_6 (1,2-butadiene) [141]; C_5H_6 (2-methyl–1-buten–3-yne) [142]; C_5H_8 (2-methyl–1,3-butadiene) [143]
Institute of Technology, Tokyo, Japan	N_2 (nitrogen) [62]; O_2 (oxygen) [71]
Instituto de Matemáticas y Fisica Fundamental, (CSIC), Madrid, Spain	N_2 (nitrogen) [63]; CH_2Cl_2 (dichloromethane) [124]; C_4H_4S (thiophene) [88]; $C_5H_4O_2$ (furfural) [89]; C_4H_8O (tetrahydrofuran) [94]; C_6H_6 (benzene) [98]; C_6H_5OH (phenol) [103]; C_5H_5N (pyridine) [105,106]; $C_4H_4N_2$ (pyrimidine) [109]; $C_4H_4N_2$ (pyrazine) [110]; $C_6H_4O_2$ (*para*-benzoquinone) [112]; $C_4H_3F_7O$ (sevoflurane) [113]
Nat. Acad. of Sciences, Uzhgorod, Ukraine	$C_6H_{12}O_6$ (fructose) [97]
Phys.-Tech. Bundesanst. Braunschweig, Germany	C_4H_8O (tetrahydrofuran) [91]; $C_4H_4O_2$ (pyrimidine) [108]
Sophia University, Tokyo, Japan	$C_6H_5CF_3$ (benzotrifluoride) [56]
Univ. College London, London, UK	H_2O (water vapor) [79]
Universidade Federal Juiz de Fora, Brazil	CH_3OH (methanol), C_2H_5OH (ethanol) [118]; C_3H_7OH (1-propanol) [119]; C_4H_9OH (1-butanol) [120]

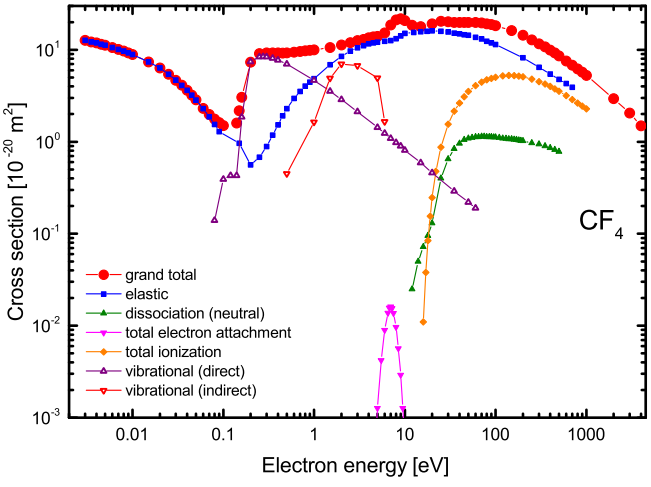

Fig. 1. Comparison of recommended *grand*-total cross section for electron scattering from CF_4 molecules with recommended and/or suggested integral cross sections for selected processes [45].

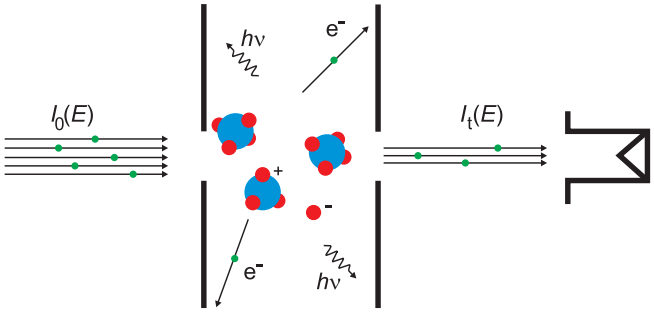

Fig. 2. The schematic of the electron transmission method.

2.1 Principles of electron transmission method

The experimental TCS data for electron scattering from molecules, presented in this short review, have been obtained in various experiments employing a transmission method. The idea of the transmission method is based on the measurements of the attenuation of a projectile beam passing through the medium under study. A schematic of the electron transmission method is illustrated in Figure 2.

The *grand*-total cross section, $Q(E)$, for the scattering of projectile particles of given energy E from target particles, is related to the attenuation of the transmitted beam intensity through the Bouguer–Beer–Lambert (BBL) formula:

$$I_t(E) = I_0(E)\exp[-Q(E)nL]\,,$$

where: $I_t(E)$ and $I_0(E)$ are the intensities of the projectile beam traversing the reaction cell taken with and without the target in the cell, respectively; n is the number density of the target, determined from the measurements of the gas/vapor target pressure and temperatures of the

scattering cell and manometer head; L stands for a path length of projectiles in the target volume.

The experimental systems used for the determination of the *grand*-total cross sections for electron scattering from atoms and molecules contain a source of electrons (thermionic filament, threshold-photoelectron, radioisotope) followed with an array of electron optics units forming electrostatic and/or magnetic fields for the controlling and guiding the beam of primary electrons. The collimated electron beam of given energy E is directed into the reaction cell filled with the gaseous or vapor sample under investigation. The target density, n, should be low enough to prevent multiple electron scattering events. Well defined impact energy and a narrow energy width of the electron beam are especially important at very low and low energies where some sharp structures in TCS may appear. Because the beam of electrons travelling a distance between an entrance and exit apertures of the scattering cell should remain well collimated, to fulfill this requirement, in some experiments the axial magnetic field is applied in the region of reaction cell. Those electrons which leave the cell through the exit aperture pass the system of the energy discriminating fields and eventually are collected in the electron detector. The solid angle subtended by the detector should be close to zero, though ensuring reasonable efficiency of the detection. All elements of the electron optics are housed in a vacuum chamber evacuated to a base pressure of about 0.1 μPa or better.

In majority of reported electron transmission experiments the quantities necessary for TCS derivation are taken directly (or determined using other measurables) and cross section values are given in absolute units, without any normalization procedure. When some quantity is difficult to determine (like the electron path length, L, across the scattering medium or the target pressure, (p), a normalization procedure is applied to put TCS values on absolute scale [56] or TCS is given in arbitrary units only.

2.1.1 Experimental problems encountered in the electron-scattering TCS measurements

The conceptually simple problem of the TCS determination through converting a few measured physical quantities according to the BBL formula becomes a quite difficult task when one wishes to fulfill all foundations of the transmission method. Because the conditions under which the BBL formula is valid are not strictly fulfilled in the real electron-transmission experiments, the measured TCS data usually systematically differ from the *true* TCSs [35]. Furthermore, there are many factors which influence the accuracy of measurables in particular transmission experiment. In consequence, distinct divergences among TCSs measured in different laboratories, which often exceed the common declared uncertainties, are visible. Some effects, which may distort the measured TCS are ever present in the transmission experiments; they are quite well identified and corresponding uncertainties can be usually reasonably estimated. More troublesome and difficult to recognize can be those factors which are associated with a specific experimental system.

A common source of the TCS uncertainty in all the electron-transmission experiments is the inevitable effusion of the target particles across orifices, through which electrons enter and leave the reaction cell. The effusion of target particles leads to inhomogeneous target distribution in the cell. At the same time, the presence of target particles just outside the cell (in the surrounding of orifices) elongates the effective path over which a notable number of scattering events may occur. In effect, the extension of the electron path length in the target can compensate, to a certain degree, the density drops near orifices. To consider this *end effect* in detail, the factor $n\,L$ in the BBL formula should be replaced with the integral $\int_a^b \mathrm{d}x n(x)$, where a and b delimit the electron pathway over which the target density $n(x)$ is high enough to influence the electron current intensity, $I(E)$. Calculations (see e.g. Ref. [57]) show that, for typical geometries of the reaction cell and the target pressures used, the end effect may distort the measured TCS up to some percent. It is also worth to note, that the target particles, which escaped from the cell into the electron optics volume (especially into the electron gun region) can alter the primary electron beam and, in consequence, influence the measured cross section. To reduce that effect, especially troublesome in the case of reactive targets, in some experimental systems the differential pumping of the electron optics volume and the surrounding of the reaction cell is applied.

More prominent contribution to the overall systematic uncertainty of TCS obtained using the transmission method comes from a finite angular discrimination against the electrons, which leave the scattering region through the exit orifice; the electron detector system does not distinguish electrons scattered into small forward angles from those not scattered. That *forward-angle scattering effect* is a common trouble in electron-transmission experiments; it leads to an overestimation of the measured transmitted electron intensity, $I_g(E)$, and hence to systematic lowering of the measured TCS with respect to its *true* value. The angular resolution problem is also related to multiple scattering and the scattering occurring in the neighborhood of scattering cell orifices. Application of energy discriminating systems, located between the scattering cell exit and the entrance to the electron detector, reduces only the number of inelastically scattered electrons which emerge from the reaction cell and might be accepted by the detector. Studies of Sullivan et al. [58] show that even small changes in the degree of the forward-angle discrimination can permanently distort the shape of the TCS energy dependence, especially at the low impact energies. Recent experiment of Kadokura et al. [79] disclosed also considerable influence of an acceptance angle of the electron detector on the magnitude of the measured low-energy TCS, particularly considerable for polar targets. One can roughly estimate the portion by which the measured TCS might be lowered due to inability to discriminate between unscattered electrons and those scattered at small angles in the forward direction. In that case, the obtained TCS values can be corrected for this effect.

For the correction, the absolute differential cross sections (DCSs) measured or calculated over the energies for which the TCS is determined and the geometry of the scattering and detection regions are indispensable. As such evaluations are rather uncertain or due to lack of appropriate DCS data are not possible, the reported experimental TCSs are usually not corrected for the forward-angle scattering effect.

Because the temperature of the reaction cell – measured in the course of the experiment – usually differs from the temperature of the manometer head, the pressure gauge readings differ from the actual target pressure. To correct for this thermomolecular pressure difference (*thermal transpiration effect*) various empirical formulas (e.g. [59–61]) are applied.

In the course of long-lasting experiments, the growing deposition of the target molecules on the electron optics elements may lead to the shift in the contact potentials and a drift in the energy scale. That becomes especially troublesome at low impact energies where sharp features in the TCS energy curve may appear and even a small drift in energy (≃0.1 eV) may cause the distinct flattening and broadening of these features and, in consequence, the loss of important information.

When the target of interest is the liquid with very low vapor pressure at room temperature, for the stabilization of vapor conditions in the reaction cell a long time is necessary, that is why the TCS uncertainty related to the difficulties in the vapor-target pressure measurement may arise.

The problems enumerated above are only the main and typical factors which can influence the accuracy of TCSs measured in the electron transmission experiments. More detailed description of error sources specific for various TCS experiments can be found in the original papers cited in the present review.

3 Experimental TCS data

In this section are presented the experimental electron-scattering *grand*-total cross sections for electron scattering from molecular targets obtained during the period 2009–2019 in the laboratories listed in Table 1. When justified, earlier TCS data are also presented to show differences in results obtained with various transmission techniques employed. Comparisons are also made to illustrate some trends visible in the TCS energy dependences when going across the target series.

3.1 Nitrogen [N_2] and oxygen [O_2]

Molecular nitrogen and oxygen, two main constituents of the Earth atmosphere, are amongst the targets which were very intensively investigated in the electron-scattering experiments. The most up-to-date measurements of electron-scattering absolute TCSs for the N_2 molecule have been carried out by Kitajima et al. [62] and Lozano et al. [63], while those for O_2 were reported very recently by Okumura et al. [71]. Experiments of Kitajima et al. and Okumura et al. have been performed

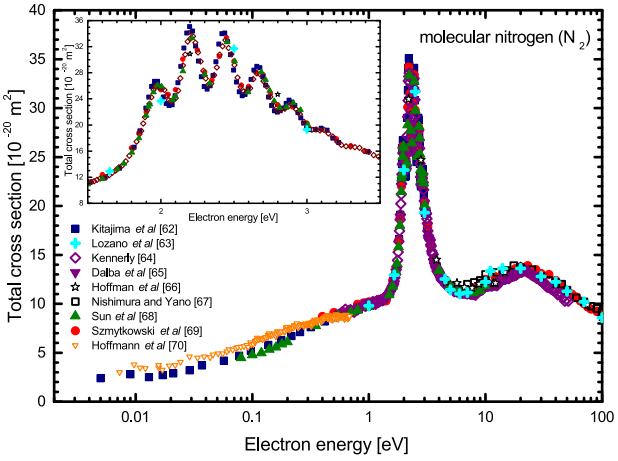

Fig. 3. Experimental *grand*-total cross section for electron scattering from N_2 molecules: recent results of Lozano et al. + [63] and Kitajima et al. ■ [62] are compared to selected earlier representative results: ◇ [64]; ▼ [65]; ☆ [66]; □ [67]; ▲ [68]; ● [69]; ▽ [70].

with an electron beam of very narrow energy width, using the threshold-photoelectron source. Lozano et al. exploited set up with a magnetically confined electron-beam [63].

Figure 3 shows electron-scattering TCS energy dependence measured for N_2 by Kitajima et al. [62] in the energy range from 5 meV to 20 eV with an electron beam of 9 meV energy width together with recent results of Lozano et al. [63] above 1 eV. Below 100 eV, for comparison depicted are also experimental TCS data obtained earlier by several groups [64–70]. In the inset, TCS results in the region of the 2.3 eV N_2^- ($^2\Pi_g$) shape resonance are shown. Due to the high-energy resolution of Kitajima et al. experiment, the location of the TCS resonant structures around 2.3 eV and 11.5 eV has been established with a good accuracy. It is worth noting, that peak positions in the 2.3 eV TCS resonant structure are often used for the calibration of the absolute energy scale of the incident electrons, therefore their precise energy location is of great importance for electron-scattering experiments. Accurate TCS values for N_2 are also useful to evaluate the reliability of novel TCS experimental setup. At very low electron-impact energies, the recent TCS findings of Kitajima et al. are consistently lower than those reported earlier by Hoffmann et al. [70], measured also with very high energy resolution.

Figure 4 presents the absolute TCSs for electron scattering from O_2 molecules in the energy range from 16 meV to 20 eV measured by Okumura et al. [71], with an electron energy width of 7 meV.

For comparison, in Figure 4 included are previous TCS results measured in other laboratories [69,72–78]. Distinct disaccord in the magnitude of TCSs obtained by different experimental groups is visible for impact energies beyond 1 eV. Inset shows the experimental TCS data for the electron–O_2 scattering below 1 eV, in the range of low-energy resonances. It is evident that, with respect to the magnitude and energy position of TCS peaks, related

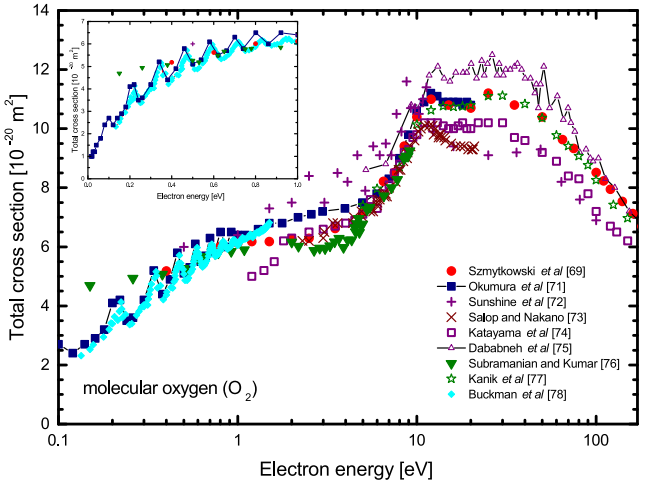

Fig. 4. Experimental *grand*-total cross section for electron scattering from molecular oxygen (O_2): the recent results of Okumura et al. –■– [71] are compared to selected earlier data: + [72]; ×[73]; □ [74]; –△– [75]; ▼ [76]; ☆ [77]; ● [69]; ◆ [78].

to the O_2^- ($^2\Pi_g$) resonant states, very low-energy results of Okumura et al. [71] are consistent with those of Buckman et al. [78], collected earlier using time-of-flight technique of 2–10 meV energy resolution.

3.2 Water [H_2O]

Interactions between electrons and water molecules are of continuous interest over the years because electron-induced processes in the media comprising water are of fundamental importance to understand life on the Earth and processes occurring in planetary atmospheres and interstellar medium. The knowledge of the efficiency of electron-water molecule interactions is also crucial for description and modeling of ionizing radiation damage to living cells and biomolecule radiolysis. For that purpose, the complete set of cross sections for particular collisional processes, including TCS data, for electron scattering from H_2O in different phases are needed and continuously updated [20,22]. Unfortunately, significant discrepancies between experimental results still exist [23,24]; they are especially distinct in the low energy region.

Very recently, Kadokura et al. [79] measured TCS in the energy range 3–300 eV, using a high-angular resolution experimental system.

Figure 5 shows their TCS results together with some selected previous TCS data [24,67,80–84] obtained in experiments using electron beams with a poorer angular discrimination. At energies below 8 eV, TCS values of Kadokura et al. are distinctly higher, by 10–100%, than all previous measurements. Such discrepancy may suggest the need of high-angular discrimination measurements in a low-energy region, especially for polar targets. Above 8 eV, results of Kadokura et al. are in very good agreement with earlier measurements of Szmytkowski and Możejko [24], while above 70–80 eV they also agree well with other TCS data presented in Figure 5.

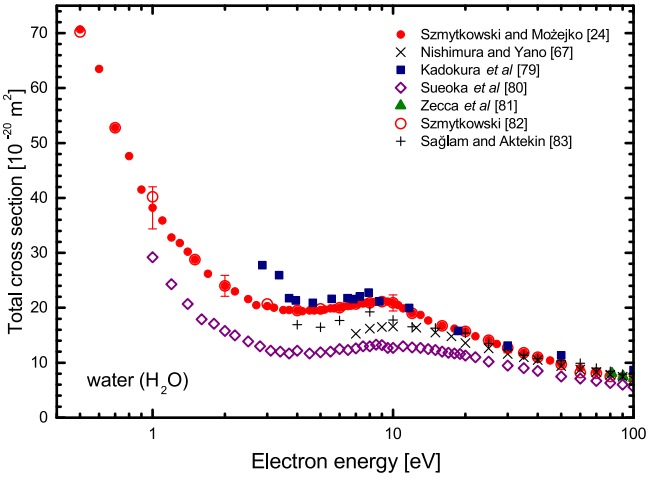

Fig. 5. Experimental *grand*-total cross section for electron scattering on water vapors (H_2O): ■ [79]; ◇ [80];▲ [81]; ○ [82]; × [67]; + [83,84], ● [24].

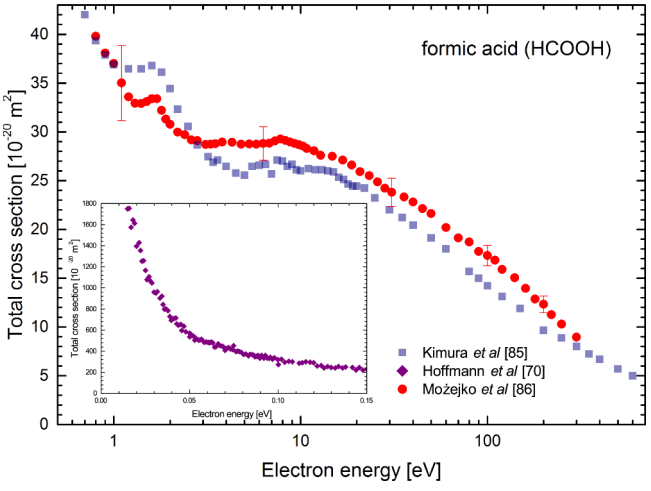

Fig. 6. Experimental *grand*-total cross section for electron scattering from formic acid (HCOOH): ■ [85]; ◆ [70]; ● [86].

3.3 Formic acid [HCOOH]

Formic acid is one of the simplest bioorganic molecule. This compound is an important intermediate in chemical synthesis and is used as a preservative and antibacterial agent. It is also considered for potential fuel cell applications. Formate group, –COOH, is a component of more complex biomolecules, including amino acids. Furthermore, formic acid is expected to play a key role in the interstellar formation of bigger biomolecules as acetic acid and glycine.

Figure 6 shows the absolute TCSs measured by Możejko et al. [86] with apparatus in which only electrostatic fields were employed for controlling the electron beam. For comparison included are previous normalized TCS results for electron scattering from HCOOH molecule derived by Kimura et al. [85] using RP-TOF technique. Both TCS energy curves are similar with respect to the shape: over all energy range investigated, the TCS for HCOOH

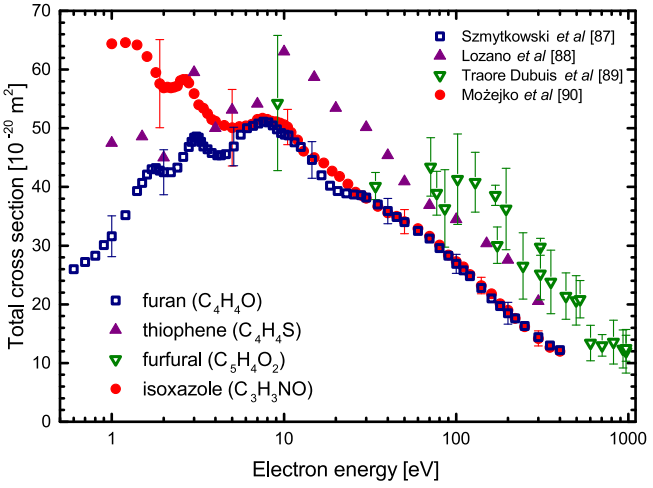

Fig. 7. Comparison of experimental *grand*-total cross sections for electron scattering from selected five-membered heterocycles: furan (C_4H_4O) □ [87]; thiophene (C_4H_4S) ▲ [88]; furfural ($C_5H_4O_2$) ▽ [89] and isoxazole (C_3H_3NO) ● [90].

systematically decreases with the energy increase. Such behavior of TCS energy function is associated with dipolar nature of the HCOOH molecule (μ_{HCOOH} = 1.4 D). At low impact energies, around 1.7 eV and 7.8 eV, resonant-like structures are visible in both TCS curves. There are, however, distinct differences in the magnitude of compared TCSs: between 1 and 3 eV results of Kimura et al. exceed those of Możejko et al., while at higher energies that relation reverses; only below 1 eV both experimental results are in very good accord. For the completeness, very low-energy TCSs of Hoffmann et al. [70], measured using the threshold-photoelectron source, are depicted in the inset; noticeable is a sharp TCS increase towards thermal energies.

3.4 Five-membered ring heterocycles

3.4.1 Furan [C_4H_4O], thiophene [C_4H_4S], furfural [$C_5H_4O_2$], and isoxazole [C_3H_3NO]

Figure 7 shows TCS energy dependences obtained in electron-transmission experiments for a class of five-membered ring heterocyclic organic compounds.

Furan [C_4H_4O] is the organic compound containing four carbon atoms and one oxygen atom as a part of the five-membered ring. It may serve as a prototype of furanose-form building block of biomolecules. Electron-scattering *grand*–total cross section for furan molecule, depicted in Figure 7, was measured by Szmytkowski et al. [87] from 0.6 to 400 eV. The TCS energy curve is dominated with very broad enhancement; on its low-energy side, distinct resonant structures are superimposed.

Thiophene molecule [C_4H_4S] has the furanose structure, however, an oxygen atom in the aromatic ring is replaced with a sulfur. Thiophene and its derivatives are widely used as building blocks in many agrochemicals and pharmaceuticals. Experimental electron-scattering TCS for thiophene was derived by Lozano et al. [88] from the attenuation of the magnetically confined electron beam in the target vapor. Both furan and thiophene molecules are weakly polar (μ_{furan} = 0.66 D; $\mu_{thiophene}$ = 0.55 D), while thiophene has distinctly higher dipole polarizability ($\alpha_{furan} = 7.2 \times 10^{-30}$ m^3; $\alpha_{thiophene} = 9.7 \times 10^{-30}$ m^3). According to the shape, the TCS curve for thiophene (see Fig. 7) closely resembles that of furan, while both TCSs distinctly differ with respect to the magnitude. The TCS values for thiophene exceed those for furan by about 20–50%, and this increase can be explained with the larger molecular size of the thiophene molecule; the size of molecule can be related to the gas-kinetic collisional cross section (σ_{gk}) which can be evaluated based on the van der Waals constant b.

Furfural [$C_5H_4O_2$] is a heterocyclic compound like its parent molecule, furan, where the hydrogen at position 2 is substituted by a functional formyl [–CHO] group. This compound is important as a substitute for petrochemical, agricultural, and pharmaceutical industries. It is considered as deoxyribose analogue – the sugar in the DNA backbone. Due to its highly asymmetric structure, the furfural molecule has a strong permanent electric dipole moment ($\mu_{furfural}$ = 3.54 D); the electric dipole polarizability of furfural ($\alpha_{furfural} = 9.9 \times 10^{-30}$ m^3) is also relatively high. TCS for electron scattering from furfural molecule was measured by Dubuis et al. [89] using an electrostatic experimental system, at the impact energies ranging from 10 to 1000 eV. Above 80 eV (see Fig. 7) the TCS for furfural is considerably higher than that for furan and thiophene; as one would expect due to larger gas-kinetic collisional cross section of furfural molecule. Somewhat intriguing is the fact, that over the energy range within 10 and 80 eV the TCS values for furfural lie in between those of its structural counterparts, furan and thiophene: $TCS_{(furan)} < TCS_{(furfural)} < TCS_{(thiophene)}$.

Isoxazole [C_3H_3NO] is a heterocyclic compound with a five-membered ring containing three carbon atoms and an oxygen atom next to the nitrogen. Isoxazole ring is a common structural fragment in biologically active molecules, it occurs in some natural products and marketed drugs. Due to its structural asymmetry, isoxazole molecule possesses a quite large electric dipole moment ($\mu_{isoxazole}$ = 2.95 D). In Figure 7 electron-scattering TCS for isoxazole molecule, measured by Możejko et al. [90], is compared with other 5-membered ring compounds. At impact energies higher than 6 eV the TCS values for isoxazole closely follow those for furan. However, in the contrast to the furan and thiophene TCS energy curves – which have the distinct enhancement with the maximum near 8 eV, the TCS energy function for isoxazole generally increases towards lower energies. Such TCS behavior can be explained in terms of much higher dipole moment of isoxazole molecule. It is worth to notice, that below 8 eV the TCS energy function for isoxazole reveals some features similar to those visible in TCS curves for furan and thiophene.

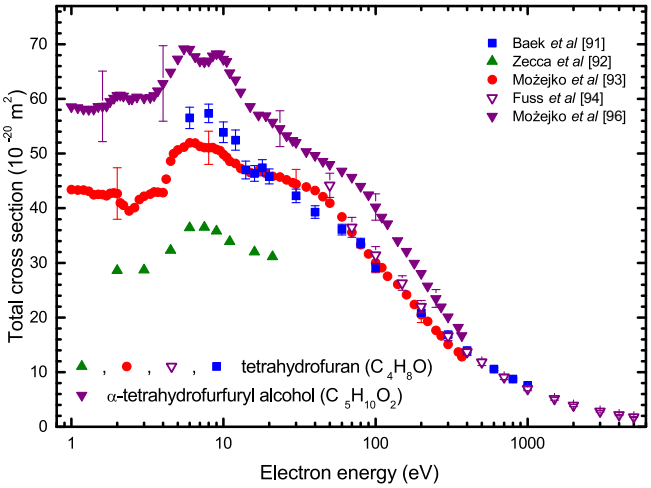

Fig. 8. Experimental *grand*-total cross sections for electron scattering from tetrahydrofuran (THF) (C_4H_8O) and α-tetrahydrofurfuryl alcohol (THFA) ($C_5H_{10}O_2$). THF: ▲ [92]; ● [93]; ▽ [94]; ■ [91]. THFA: ▼ [96].

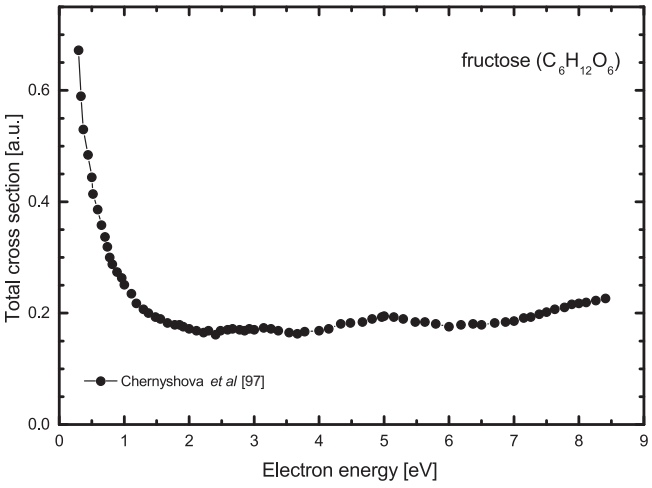

Fig. 9. Experimental *grand*-total cross section for electron scattering from fructose ($C_6H_{12}O_8$): ● [97].

3.4.2 Tetrahydrofuran (C_4H_8O) and α-tetrahydrofurfuryl alcohol [$C_5H_{10}O_2$]

Tetrahydrofuran (THF) heterocyclic molecule, with one oxygen atom in the ring, has been the subject of more electron scattering studies than any other 5-member ring compounds. It is due, in part, to the fact that THF has a structure similar to that of 2-deoxyribose, a sugar in the DNA backbone, and therefore is considered as its simple molecular analogue. THF is commonly used as a solvent and intermediate in the chemical industry.

α-tetrahydrofurfuryl alcohol (THFA) consists of a tetrahydrofuran ring substituted in the position 2 with a hydroxymethyl [CH_2OH] group. THFA is used in agriculture, manufacture of advanced electronics, and as a chemical intermediate in pharmaceutical industry. It is also being considered for use as an additive in fuels. THFA can be also treated as a close analogue of deoxyribose unit in the DNA.

Total cross section for electron scattering from THF has been measured recently by Baek et al. [91], from 6 to 1000 eV. Their results are shown in Figure 8 together with earlier experimental TCS data of Zecca et al. [92] obtained in energy range from 2 to 21 eV, Możejko et al. [93] measured between 1 and 370 eV, and Fuss et al. [94] taken within 50–5000 eV. Experimental systems used by Baek et al. and Możejko et al. are free of magnetic field, while Zecca et al. and Fuss et al. employed magnetic fields in their electron spectrometers.

Figure 8 shows that while the energy dependence of all depicted TCSs for THF molecule is quite similar, differences in the magnitudes are appreciable. In the region of the main TCS maximum, between 6 and 12 eV, recent results of Baek et al. lie about 10% above earlier data of Możejko et al. while between 30 and 50 eV a relation of both curves reverses. The magnitude of TCS obtained by Zecca et al. is systematically much lower than that of Możejko et al. and Baek et al., across the common energy range. It is probably due to high energy dispersion of electron beam in the Trento experiment.

For comparison, in Figure 8 TCS results for THFA molecule measured by Możejko et al. [96] are also included. Figure 8 reveals that with respect to the shape, TCS energy function for α-tetrahydrofurfuryl alcohol looks similar to that for tetrahydrofuran. Due to the presence of hydroxymethyl group in THFA compound, TCS values for THFA are distinctly higher than those for THF molecule over the whole energy range investigated.

3.4.3 Fructose [$C_6H_{12}O_6$]

In Figure 9 depicted is TCS for the electron scattering from fructose molecules over collisional energies ranging from about 0.3 to 8.5 eV. The experiment was performed by Chernyshova et al. [97] using hypocycloidal spectrometer.

Measured cross section was reported in arbitrary units only due to inability to estimate of the fructose vapor pressure in the reaction cell. Below 1 eV, the TCS energy curve rises very sharply towards the lowest energies applied. Two weak resonant-like structures in the TCS curve are discernible around 3 and 5 eV, respectively.

3.5 Six-membered ring heterocycles

In this section we present electron-scattering *grand*–total cross sections measured recently for benzene and heterocyclic compounds structurally related to benzene with one or two carbon atoms in the ring replaced by a nitrogen or oxygen atom. Experimental TCS energy dependences for benzene derivatives in which a hydrogen atom in position 2 is substituted by a functional group (OH, CH_3 or CF_3) are also included.

Benzene-derived units occur in many compounds of biological importance. They are used as precursors to agrochemicals and pharmaceuticals and as reagents and

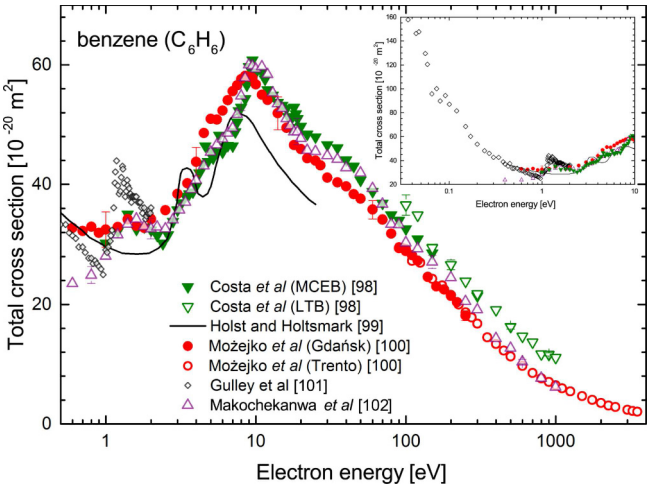

Fig. 10. Experimental *grand*-total cross section for electron scattering from benzene (C_6H_6): — [99]; ● (Gdańsk) [100]; ○ (Trento) [100]; ◇ [101];△ [102]; ▼ MCEB [98]; ▽ LTB [98].

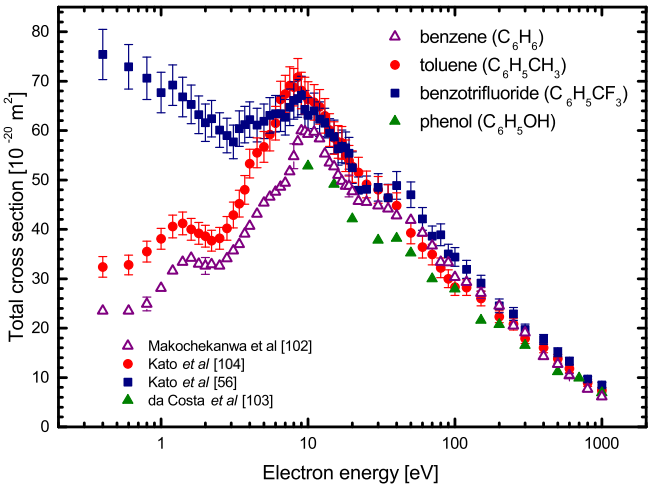

Fig. 11. Experimental *grand*-total cross sections for selected benzene derivatives: phenol (C_6H_5OH) ▲ [103]; toluene ($C_6H_5CH_3$) ● [104]; and trifluoromethyl-benzene ($C_6H_5CF_3$) ■ [56]. For comparison TCS for benzene is also included: (C_6H_6) △ [102].

solvents. To reduce the amounts of these compounds, released in technological processes to the environment, some technologies are proposed in which the electron-scattering data are essential for modeling processes to remove these compounds from the waste stream.

3.5.1 Benzene and its mono-substituted derivatives: phenol [C_6H_5OH], toluene [$C_6H_5CH_3$] and trifluoromethyl-benzene [$C_6H_5CF_3$]

Figure 10 shows total cross section for electron scattering from the benzene molecule measured recently by Costa et al. [98] over wide energy range: from 1 to 200 eV, using magnetically confined electron transmission beam (MCEB); and from 100 to 1000 eV with the linear electrostatic transmission beam system (LTB). For comparison pioneering results of Holst and Holtsmark [99], and those more modern of Możejko et al. [100], Gulley et al. [101] and Makochekanwa et al. [102], obtained with various transmission techniques, are also included.

Figure 10 demonstrates that presented TCS energy dependences are in satisfactory agreement with respect to the shape. Only around 1 eV, the TCS energy curve of Gulley et al. differs from others: due to much better energy resolution of their experiment, the resonant structure in their TCS curve appears to be more expressive and complex. More distinct discrepancies are visible in the TCS magnitudes. Above 400 eV, the very recent results of Costa et al. are higher by about 30–40% than previous TCS data [100,102], probably due to the worse angular resolution of earlier experiments. Above the 10 eV maximum, the earliest results of Holst and Holtsmark lie distinctly below later measurements. Below 10 eV, except the energy range below 2 eV, differences in magnitude do not exceed declared uncertainties. Inset shows that below 1 eV the TCS for benzene, the nonpolar molecule, rises sharply towards thermal energies.

Figure 11 presents electron-scattering TCSs for mono-substituted benzene-derived compounds: phenol [C_6H_5OH], toluene [$C_6H_5CH_3$], and trifluoromethyl-benzene [$C_6H_5CF_3$] – the compounds in which one hydrogen atom in benzene ring is substituted with the OH, CH_3, or CF_3 unit, respectively.

Phenol [C_6H_5OH] rings are common in nature; they represent a prototype subunit for lignin. The compound is used as intermediate for industrial organic synthesis, it has also medical applications. Toluene [$C_6H_5CH_3$] occurs naturally in crude oil and is also detected in smoke from cigarettes and wood (it belongs to the dangerous neurotoxins). The compound is exploited extensively as starting material in the manufacturing of industrial chemicals and pharmaceuticals. It is also applied as a common solvent and as a fuel additive. Trifluoromethyl-benzene [$C_6H_5CF_3$] is used as an alternative solvent for organic and fluorous synthesis.

Electron-scattering TCS for phenol, from low to intermediate energies, has been measured by da Costa et al. [103] using an electron-transmission apparatus based on a magnetic confinement of an electron beam. Cross sections for toluene and trifluoromethyl-benzene were obtained by Kato et al. [56,104] with a retarding potential time-of-flight (RP-TOF) method, in which a guiding magnetic field was applied. To examine how the attachment of different groups to benzene ring influences the electron scattering (the *substitutional effect*), the results for benzene derivatives are compared with previous TCS data for benzene obtained with the same RP-TOF experimental system [102]. Figure 11 shows that above 10 eV all depicted TCS energy curves are similar in the shape. Some differences (10–20%) with respect to the magnitude can be explained in terms of the various molecular size of considered targets. At low impact energies, below 10 eV, differences among TCS magnitudes for benzene derivatives become more significant – the TCS values

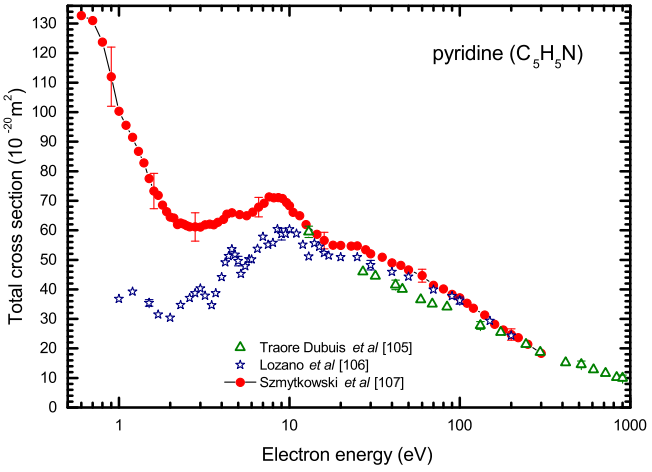

Fig. 12. Experimental *grand*-total cross section for electron scattering from pyridine (C_5H_5N): △[105]; ☆ [106]; —●— [107].

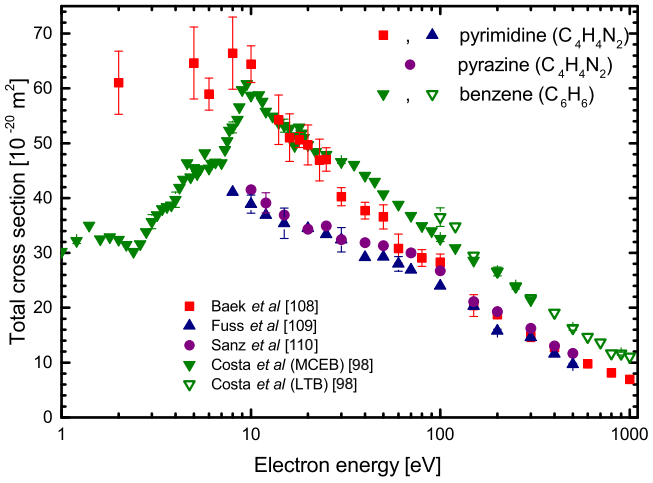

Fig. 13. Experimental *grand*-total cross sections for electron scattering from pyrimidine ($C_4H_4N_2$) and pyrazine ($C_4H_4N_2$). Pyrimidine ■ [108]; ▲ [109]. Pyrazine: ● [110]. For comparison TCS for benzene is shown: ▼ (MCEB); ▽ (LTB) [98].

for toluene and benzene decrease rapidly with decreasing energy, while TCS for trifluoromethyl-benzene distinctly increases. This is, in part, due to different values of electric dipole moments of considered compounds: benzene molecule does not possess permanent electric dipole moment ($\mu_{C_6H_6}$ = 0 D), toluene is only slightly polar ($\mu_{C_6H_6CH_3}$ = 0.375 D), while the trifluoromethyl-benzene molecule has the significant permanent dipole moment ($\mu_{C_6H_5CF_3}$ = 2.86 D). It is also worth noting that features visible in compared TCS curves are located around the same impact energies.

3.5.2 Pyridine [C_5H_5N]

The pyridine units occur in numerous compounds of biological importance, e.g. in nicotine and B-group vitamins. The pyridine compound is used as a precursor to agrochemicals and pharmaceuticals and as a solvent and reagent. Pyridine derivatives have also an importance for modern clinical applications.

TCS energy dependences depicted in Figure 12 present results for pyridine measured recently by Dubuis et al. [105], Lozano et al. [106], and Szmytkowski et al. [107] over wide electron impact energy range. TCS results of Dubuis et al. and those of Szmytkowski et al. were obtained using electron-transmission systems with electric fields only, while Lozano et al. employed a magnetic field for the electron-beam confinement. Figure 12 shows that, in the common energy range of those experiments, all presented TCS energy curves are in a reasonable agreement according to the shape, although distinct differences exist in the TCS magnitude at low impact energies, especially below 10 eV. Below 2.5 eV, TCS values of Szmytkowski et al. rapidly increase with decreasing energy – as one would expect for polar molecule ($\mu_{pyridine}$ = 2.22 D), while the TCS obtained by Lozano et al. rather oscillates. This discrepancy is probably related to the detection a portion of the scattered electrons in the Lozano et al. experiment, due to quite large acceptance angle of their electron detector. On the other hand, it is clearly visible that in the experiment of Lozano et al. the resonant features are much more perceptible.

3.5.3 Pyrimidine and pyrazine [$C_4H_4N_2$]

Pyrimidine and a pyrazine are heterocyclic organic compounds similar to benzene in which two carbon atoms are replaced by nitrogen atoms; in pyrimidine the substituted nitrogen atoms are located at positions 1 and 3 of the six-membered ring, while in pyrazine at positions 1 and 4. Pyrimidine is considered as the model of building blocks of several biological molecules and DNA/RNA nucleobases (thymine, cytosine and uracil). Therefore, it constitutes a convenient model system for explaining electron scattering properties of biomolecules.

Experimental data for both isomers are presented in Figure 13 together with very recent TCS data for benzene [98] for comparison. Cross sections for pyrimidine were measured with two quite different electron-transmission experimental systems. Results of Baek et al. [108] were obtained with the apparatus in which magnetic field along the electron trajectory was highly reduced, while those of Fuss et al. [109] were taken with a system, in which an electron beam was magnetically confined. Above 60 eV, both TCS data sets are very similar, while at lower energies results of Baek et al. distinctly exceed those of Fuss et al.; near 10 eV the difference exceeds even 50% and such a high disaccord is somewhat intriguing. However, it is worth to mention, that in the low energy range also TCS results of Baek et al. [91] for tetrahydrofuran (see Fig. 8) are higher by about 10% than those of Możejko et al., measured using a magnetic field-free apparatus.

TCS results for pyrazine were obtained by Sanz et al. [110] with the same apparatus as that used in the experiment with pyrimidine [109]. Pyrazine is a structural isomer of pyrimidine molecule with very similar electric

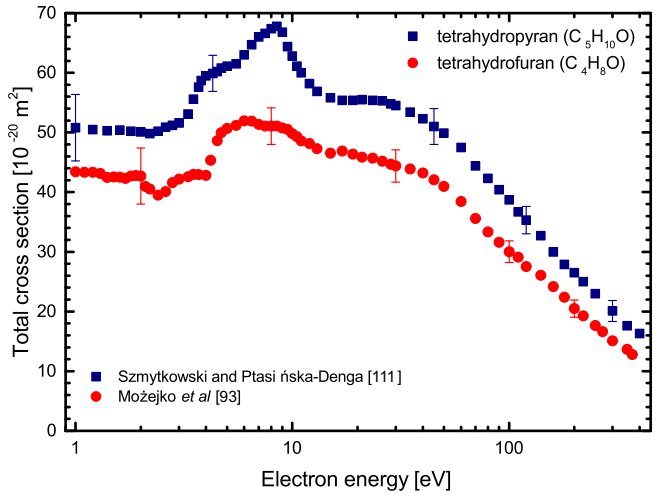

Fig. 14. Experimental *grand*-total cross section for electron scattering from tetrahydropyran ($C_5H_{10}O$): ■ [111]. For comparison TCS for electron scattering from tetrahydrofuran (THF) is also shown: ● [93].

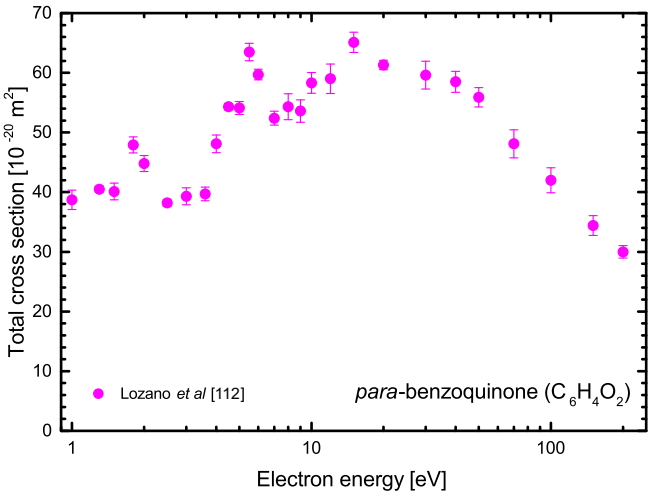

Fig. 15. Experimental *grand*-total cross section for electron scattering from *para*-benzoquinone ($C_6H_4O_2$): ● [112].

polarizability (~9×10^{-30} m^3) and, due to its symmetrical structure, has no permanent electric dipole moment (μ_{pyridine} = 0 D), while pyrimidine is rather highly polar molecule ($\mu_{\text{pyrimidine}}$ = 2.33 D).

In spite of an essential difference in values of electric dipole moments of both $C_4H_4N_2$ isomers, the TCS energy dependence for pyrazine molecule measured by Sanz et al. appears to be very similar in the shape and magnitude to that for pyrimidine obtained by Fuss et al. [109], over the whole energy range applied. Above 100 eV, TCS results of Sanz et al. for pyrazine are also in accord with data of Baek et al. [108] for pyrimidine.

Cross sections for both $C_4H_4N_2$ isomers of Sanz et al. and Fuss et al. are distinctly lower than TCSs for benzene measured by Costa et al. [98], in the same laboratory. On the other hand, TCS values for pyrimidine, measured by Baek et al., are below 10 eV much higher than those for benzene, nearly equal to them between 10 and 20 eV, and then lie well below benzene curve.

3.5.4 Tetrahydropyran [$C_5H_{10}O$] and *para*-benzoquinone [$C_6H_4O_2$]

Tetrahydropyran (THP) consists of a saturated six-membered ring containing five carbon atoms and one oxygen. The compound is commonly used in organic synthesis. Sugars often occur in pyranose forms containing the tetrahydropyran ring; the THP ring is also the core of glucose.

Figure 14 shows TCS for electron scattering from THP measured from 1 to 400 eV by Szmytkowski and Ptasińska-Denga [111]; The TCS for tetrahydrofuran (THF), measured with the same experimental system, is also depicted for comparison. According to the shape, TCS energy curve for THP reminds somewhat that for THF. The magnitude of TCS for THP exceeds distinctly that for THF compound, over the whole energy range applied. Note, that also the gas-kinetic scattering cross section for THP is larger than that for THF molecule.

Para-benzoquinone (*p*BQ) compound, is used in organic chemistry as an oxidizing agent. Its derivatives show a biological and/or pharmaceutical activity. Figure 15 depicts TCS for electron scattering from the $C_6H_4O_2$ molecule measured recently from 1 to 200 eV by Lozano et al. [112].

Very broad TCS enhancement peaking around 16 eV is superimposed with two distinct resonant-like features located near 2 and 5.5 eV, respectively. It is interesting, that there is some similarity in the shape and to lesser degree in magnitude of TCSs for pyridine and *para*-benzoquinone (see Figs. 12 and 15).

3.6 Sevoflurane [$C_4H_3F_7O$]

Sevoflurane is commonly used as an inhalational anesthetic. Figure 16 shows TCS energy dependence for electron scattering from $C_4H_3F_7O$ molecule measured by Lozano et al. [113] from 1 to 300 eV, with the experimental setup that makes use of a strong axial magnetic field.

Two observations concerning TCS for sevoflurane are worth noting: (i) the TCS sharply decreases with the energy decrease towards 1 eV – it is somewhat unusual trend for highly polar targets ($\mu_{\text{sevoflurane}}$ = 2.3 D); (ii) the very broad intermediate-energy hump, peaking near 40–50 eV, is clearly visible – that TCS structure is characteristic for highly fluorinated compounds (e.g. Refs. [114,115]), see also Figure 17.

3.7 Acetaldehyde [H_3C–COH], acetone [$(CH_3)_2CO$], and hexafluoroacetone [$(CF_3)_2CO$]

In Figure 17 collected are absolute electron-scattering TCS energy dependences for compounds with the carbonyl (>C=O) group. To keep conformity, all displayed TCS results are taken from experiments performed in the same laboratory [116,117].

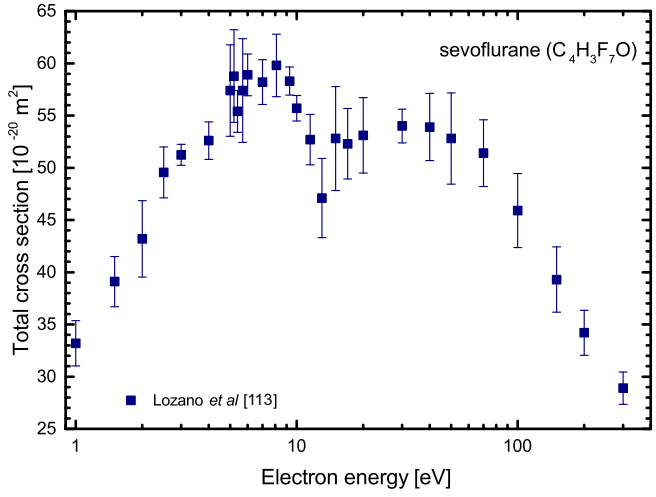

Fig. 16. Experimental *grand*-total cross section for electron scattering from sevoflurane ($C_4H_3F_7O$): ■ [113].

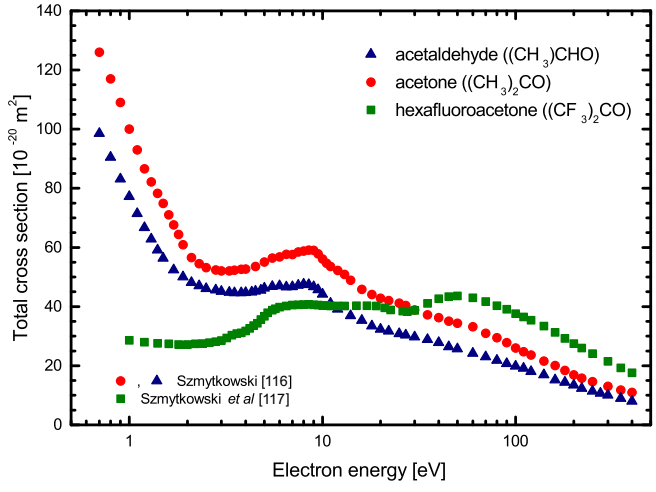

Fig. 17. Comparison of experimental *grand*-total cross sections for acetone ● [116]; acetaldehyde ▲ [116]; and hexafluoroacetone ■ [117].

Comparison of TCSs for acetone [$(CH_3)_2CO$] and acetaldehyde [H_3C–COH] shows that replacing one hydrogen atom in [H_3C–COH] by the methyl group to form acetone [$(CH_3)_2CO$] increases the magnitude of TCS; the shape of the curves is almost similar. In addition, comparison of TCS curves for the acetone [$(CH_3)_2CO$] and hexafluoroacetone [$(CF_3)_2CO$] molecules exhibits how the replacement of hydrogen atoms with fluorine reflects in the electron-scattering cross sections. It is evident that the fluorination significantly changes the electron interaction with molecules over the entire energy range studied. Fluorine atoms substituted for hydrogens essentially change the electric charge distribution: $\mu_{\text{acetone}} = 2.88$ D, $\mu_{\text{hexafluoroacetone}} \simeq 0.4$ D. In consequence, below 10 eV, the TCS for $(CH_3)_2CO$ is drastically higher than that for $(CF_3)_2CO$, while above 30 eV relation between compared TCSs reverses – the TCS for hexafluoroacetone becomes consistently higher, with very broad hump centered near

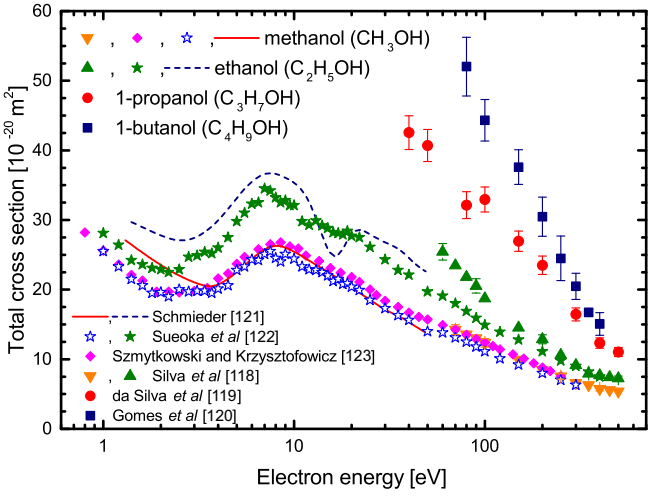

Fig. 18. Experimental *grand*-total cross section for electron scattering with primary alcohols $C_nH_{2n+1}OH$, $n = 1-4$. Methanol (CH_3OH): — [121]; ☆ [122]; ◆ [123]; ▼ [118]. Ethanol (C_2H_5OH): — [121]; ★ [122]; ▲ [118]. 1-propanol (C_3H_7OH): ● [119]. 1-butanol (C_4H_9OH): ■ [120].

50 eV. The appearance of such a broad hump located between 20 and 100 eV in the TCS energy curve is typical for fluorinated compounds (cf. Fig. 16).

3.8 Linear primary alcohols: $C_nH_{2n+1}OH$, $n = 1$–4

Alcohols are among the most common organic compounds. They are used in synthesis of other chemicals, in pharmaceuticals and as solvents. Because alcohols are also used as additions to fuels, their interaction with electrons in scattering processes is important for modeling alcohol combustion through a spark ignition within an engine.

Figure 18 shows electron-scattering TCSs for homologous series of linear primary alcohols: methanol, ethanol, 1-propanol, and 1-butanol ($C_nH_{2n+1}OH$, n = 1–4), measured recently by Silva et al. [118,119] and Gomes et al. [120] at intermediate impact energies using the same apparatus; some previous experimental TCS results [121–123] are also included for comparison. At energies above 250 eV, TCS measurements of Silva et al. for ethanol agree well with respect to the magnitude with earlier data of Sueoka et al. [122], being distinctively higher at lower energies.

Based on TCS results for alcohol series ($C_nH_{2n+1}OH$, n = 1–4), Gomes et al. [120] derived the formula which relates the intermediate-energy TCS of alcohol molecules to the respective electric dipole polarizability. The formula indicates the role of a spatial spread of a molecular charge cloud in the scattering process. It can be utilized to derive TCSs for larger members of this alcohol family.

3.9 Dichloromethane [CH_2Cl_2]

Dichloromethane (DCM) is an organic compound widely used as a solvent for many chemical processes. Though,

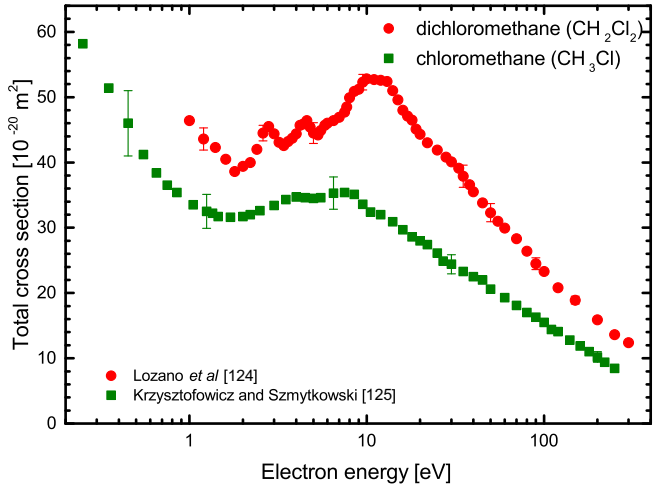

Fig. 19. Comparison of experimental *grand*-total cross sections for dichloromethane ● [124] and chloromethane ■ [125].

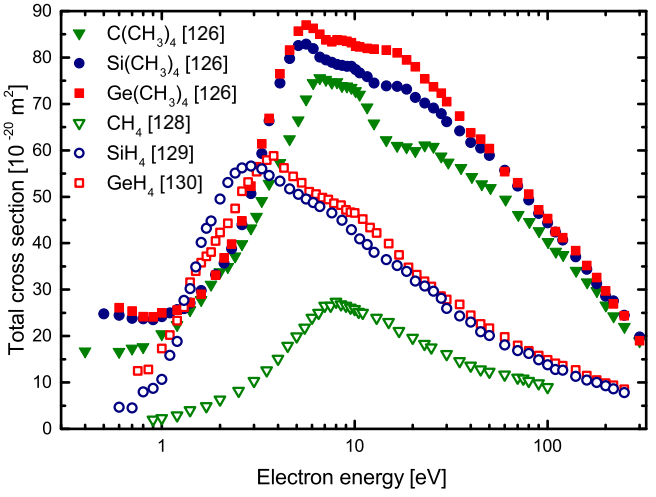

Fig. 20. Experimental *grand*-total cross section for electron scattering from tetramethylmethane ($C(CH_3)_4$) ▼ [126], tetramethylsilane ($Si(CH_3)_4$) ● [126], and tetramethylgermane ■ ($Ge(CH_3)_4$) [126] compared to TCS for methane (CH_4): ▽ [128]; silane (SiH_4) ○ [129], and germane (GeH_4) □ [130].

the majority of dichloromethane in the environment comes from industrial emissions, there are also its natural sources.

Figure 19 depicts electron-scattering absolute *grand*-total cross section for the CH_2Cl_2 molecule measured by Lozano et al. [124] over the energy range 1–300 eV. To examine how the substitution of hydrogen atoms with chlorine in methane molecule reflects in the TCS energy dependence, in Figure 19 TCS results for chloromethane [125] are also included. In general, both TCS energy dependences are similar with respect to the shape, when TCS values for CH_2Cl_2 are consistently higher. Below 2 eV, TCS curve for CH_2Cl_2 and that for CH_3Cl rise towards lower energies; such behavior is typical for target molecules possessing significant electric dipole moment, $\mu_{CH_2Cl_2}$ = 1.6 D and μ_{CH_3Cl} = 1.9 D. Two distinct resonant-like structures in TCS energy curve for CH_2Cl_2 are visible in the vicinity of 2.8 and 4.4 eV, followed with the broad maximum located near 10 eV; they are only weekly marked in TCS for CH_3Cl.

3.10 Tetrahedral compounds

Recently, *grand*-total cross sections for electron scattering from series of $X(CH_3)_4$ compounds (where X=C, Si, and Ge) have been measured by Stefanowska-Tur et al. [126], and for $SnCl_4$ by Możejko et al. [127]. All those compounds can be used in the focused electron beam induced deposition technique (FEBID) as precursors of conducting or semiconducting nanostructures.

Figure 20 shows electron-scattering TCSs for tetramethylmethane, tetramethylsilane and tetramethylgermane measured at low and intermediate impact energies by Stefanowska et al. [126]. For comparison also TCS data for XH_4 (X=C, Si, Ge) compounds, obtained in the same laboratory [128–130], are shown in this figure. It can be seen in Figure 20 that the replacement of the hydrogen atoms in XH_4 molecules with the CH_3 groups reflects in the energy shift of the main TCS maximum. Above 10 eV, the amplitudes of TCS features observed for permethylated compounds are significantly higher than those for XH_4 targets. That is consistent with earlier observation of Szmytkowski et al. [131] that external rather than central atoms have stronger influence on the energy dependence of the TCS for tetrahedral compounds.

Grand-total cross section for electron collisions with tin tetrachloride [$SnCl_4$] molecules measured for electron energies ranging from 0.6 to 300 eV [127] is shown in Figure 21 together with TCS data for carbon tetrachloride, (CCl_4 [132]), silicon tetrachloride ($SiCl_4$ [133]) and germanium tetrachloride ($GeCl_4$ [129]); TCS for $SnCl_4$ has considerably higher magnitude over the entire investigated energy range. All TCS energy curves presented in Figure 21 have distinct low-energy resonant maximum located between 0.9 and 2 eV. It was shown that in the case of $SnCl_4$ this feature can be composed of two narrow resonant states located at around 0.94 eV and 1.64 eV [127]. At higher collisional energies, where resonant processes are not so important, the TCS magnitude for compared molecules increases with the size of the central atom in target molecule.

3.11 Hydrocarbons

3.11.1 Ethylene derivatives

Figure 22 shows TCS energy dependences for electron scattering from ethylene [$H_2C{=}CH_2$] molecule and its methyl-substituted derivatives (propene [$H_2C{=}CHCH_3$], 2-methylpropene [$H_2C{=}C(CH_3)_2$], 2-methyl–2-butene [$(H_3C)HC{=}C(CH_3)_2$] and 2,3-dimethyl–2-butene [$(H_3C)_2C{=}C(CH_3)_2$]), in which the methyl groups [CH_3] are attached to the C=C double bond replacing the successive hydrogen atoms. To keep conformity, all displayed

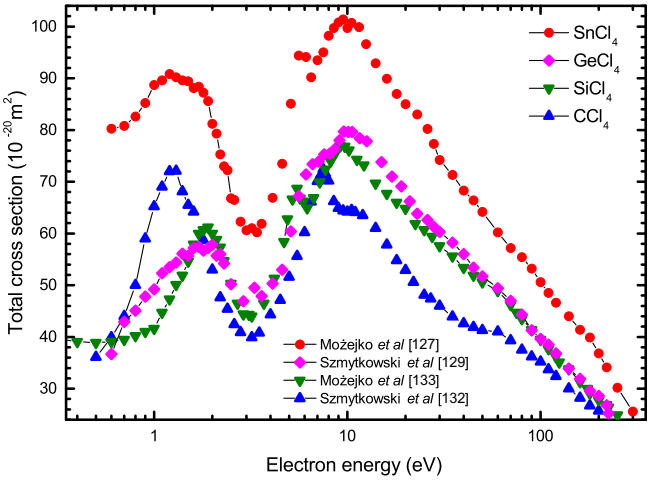

Fig. 21. Experimental *grand*-total cross section for $SnCl_4$ molecules —●— [127] compared with TCS for: CCl_4 —▲— [132]; $SiCl_4$ —▼— [133]; $GeCl_4$ —◆— [129]

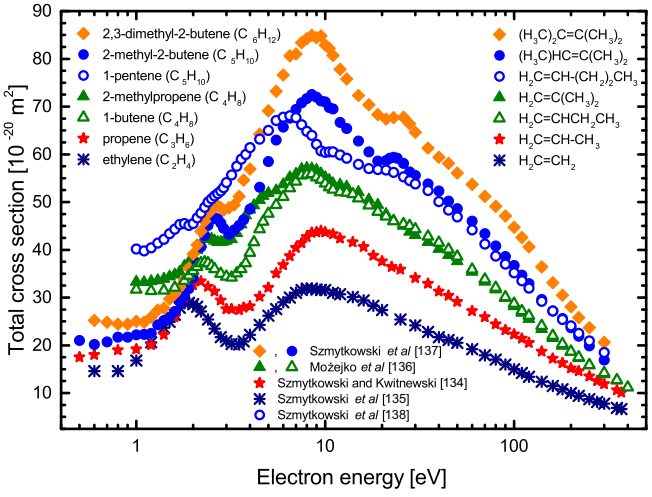

Fig. 22. Comparison of experimental *grand*-total cross sections for electron scattering from ethylene ✳ [135]; propene ★ [134]; 1-butene △ [136]; 2-methylpropene ▲ and 1-pentene ○; [138]; 2-methyl-2-butene ● [137]; 2,2-dimethyl-2-butene ◆ [137].

TCS results are taken from experiments performed with the same experimental setup [134–137]. In general, the compared TCS curves show very similar behavior over the whole investigated energy range. Figure 22 also reveals that as the number of methyl groups in target molecule increases the position of the low-energy resonant peak shows a steady shift in energy and its amplitude tends to be less pronounced. Moreover, in TCS some new structures become more visible in the vicinity of 20 eV.

In Figure 22 TCS energy curves for 1-butene [H_2C=$CHCH_2CH_3$] (from Ref. [136]) and 1-pentene [H_2C=CH-$(CH_2)_2CH_3$] (from Ref. [138]) measured with the same apparatus are also included. Those two alkenes, together with propene C_3H_6 constitute a family of ethylene straight-chain derivatives. In the successive members of this family a functional unit of increasing length is attached to the C=C double bond replacing the same hydrogen atom in the parent H_2C=CH_2 molecule. The general similarity in the shape of TCS curves for the series of ethylene straight-chain derivatives is visible. The magnitude of the TCS for members of a series increases with the increasing length of the substituent unit. Above 30 eV, the increase of the TCS at the given energy is nearly the same when going across the investigated series of targets. It suggests that the impinging electron of intermediate and of high impact energy perceives the molecule rather as an aggregate of individual atoms. The effect of the arrangement of atoms in the target molecule on the TCS energy dependences is visible for two isomers of the C_4H_6 compound: 1-butene and 2-methylpropene; as well as for isomers of C_5H_{10}: 1-pentene and 2-methyl–2-butene. This *isomeric effect* is more noticeable at lower impact energies.

3.11.2 Acetylene derivatives

Figure 23 presents TCS energy curves for acetylene [HC≡CH] and 1-butyne [HC≡C-CH_2CH_3] molecules

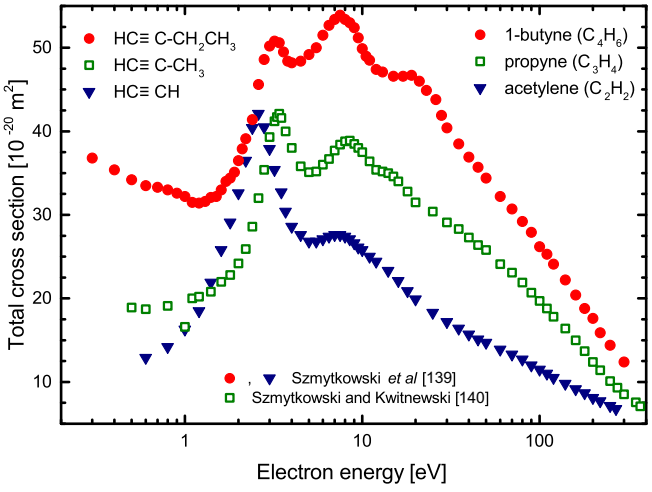

Fig. 23. Comparison of experimental *grand*-total cross sections for electron interactions with selected alkynes: acetylene ▼ [139]; propyne □ [140]; 1-butyne ● [139].

measured [139] in the low and intermediate impact energy range. To examine how replacement of one hydrogen atom in the acetylene molecule with various functional groups reflects in the TCS energy dependence, the TCS energy curves for C_2H_2 and C_4H_6 are compared with the previous TCS data for propyne [HC≡C–CH_3], obtained with the same technique [140]. Referring to Figure 23, one can see that there is a close similarity in the shape of TCS curves for the compared series of alkynes. Generally, the magnitude of TCS increases with the increasing length of the functional unit replacing one hydrogen atom in the HC≡CH molecule. The exception is the first TCS resonant peak – its amplitude decreases with the increasing size of the target molecule. In the vicinity of 20 eV, a shoulder appears for the homologues of acetylene; such

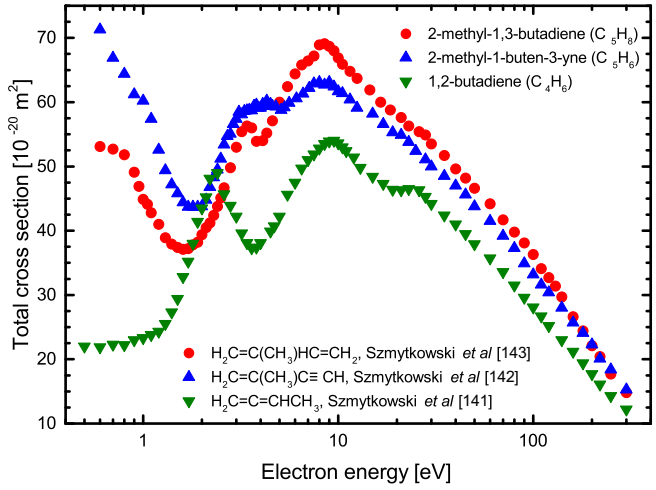

Fig. 24. Experimental *grand*-total cross section for electron scattering from 1,2-butadiene (C_4H_6) ▼ [141]; 2-methyl-1-buten-3-yne (C_5H_6) ▲ [142] and 2-methyl-1,3-butadiene (C_5H_8) ● [143].

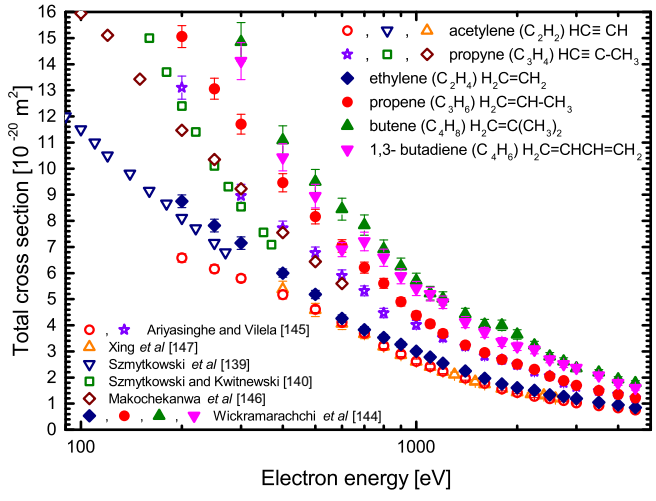

Fig. 25. Comparison of high-intermediate energy experimental *grand*-total cross sections for family of alkene molecules [144] and simple alkynes molecules [145]. Alkenes: ethylene ◆; propene ●; butene ▲; 1,3-butadiene ▼ [144]. Alkynes: acetylene: ○ [145]; ▽ [139]; △ [147] and propyne: ☆ [145]; ◇ [146]; □ [140].

substitutional effect was also visible for substituted alkenes (see Fig. 22).

3.11.3 Miscellaneous

In this section recent absolute electron-scattering TCSs for molecules with two C=C double bonds (2-methyl–1,3-butadiene [$H_2C{=}C(CH_3)HC{=}CH_2$] (C_5H_8) and 1,2-butadiene [$H_2C{=}C{=}CHCH_3$] (C_4H_6)) and the molecule with one C=C double and one C≡C triple bond (2-methyl–1-buten-3-yne [$H_2C{=}C(CH_3)C{\equiv}CH$] ($C_5H_6$)) are presented.

Grand-total cross sections for C_4H_6 [141], C_5H_6 [142] and C_5H_8 [143] molecules were measured with the same electron-transmission setup in the Gdańsk laboratory. 2-methyl–1,3-butadiene (isoprene) constitutes the building block of natural rubber, terpenes and important biological compounds such as a chlorophyll or vitamin A. It occurs in the environment as emissions from vegetation and as a by-product in a large-scale petrochemical industry. 1,2-butadiene compound is used primarily in polymer and chemical industry. The 2-methyl–1-buten-3-yne molecules arose as the reaction product in the experiments in which gas mixtures representative of Titan's atmosphere were irradiated with UV light or subjected to electrical discharges.

Figure 24 shows that above 2 eV a general energy dependence of compared cross sections is similar. Differences in the TCS magnitude are especially appreciable at energies below 20 eV, where the structure of the target molecule seems to play an essential role in the electron scattering. Above 30 eV, TCSs for compared targets have similar trend – they decease with increasing energy.

3.11.4 High-intermediate energies

Majority of recently measured total cross sections was obtained at low and low-intermediate energies. Wickramarachchi et al. [144] measured electron-scattering TCSs for group of alkene molecules in the energy range from 200 to 4500 eV. Their experimental results were used as the basis for the development of an empirical expression for the energy variation of TCS for chain-like hydrocarbons with C–C single and C=C double bonds. To account for the variation of TCS in the presence of triple bonded carbon atoms, Ariyasinghe and Vilela extended high-energy measurements of TCSs to simple alkynes (acetylene and propyne) [145]. Figure 25 collects TCS results from both experiments [144,145]. In the same figure earlier cross sections for acetylene and propyne [139,140,146,147], extending TCS towards lower energies (below 200 eV), are also depicted for comparison.

Based on both TCS data sets [144,145], Ariyasinghe and Vilela derived a new empirical formula which relates TCSs for selected normal hydrocarbons to electron impact energy, the number of hydrogen atoms and the number of single, double, and triple bonded carbon atoms in the target molecule. Cross sections calculated using that formula reproduce reasonably well the experimental TCS findings above 200 eV. Below 200 eV, the estimated this way cross sections are distinctly higher than the available experimental TCS results.

4 Final remarks

During the last decade (2009/2010–2019) total cross sections for electron scattering from over 40 targets have been measured in various laboratories using electron transmission technique; the employed electron-transmission systems differed in their construction and operating conditions. It should be pointed out, however, that some

of those experimental groups ceased TCS measurements in the latter half of that period. The experiments have been focused mainly on the molecular targets of biological, astrobiological and technological interest, what reflects the trend in other spectroscopic studies. In general, TCS functions obtained in different laboratories are in general qualitative agreement, however, they often differ significantly in the magnitudes, mainly at low collisional energies. In some cases, the measured TCS energy dependences differ also in peak positions. For some targets fragmentary energy ranges have been studied so far and only one experimental TCS energy curve is available.

For the future, to resolve discrepancies, mentioned above, further TCS measurements are necessary. At low collisional energies, especially for polar targets and for molecules for which low-energy resonant states exists, the essential improvements in the TCS quality depends mainly on the electron-beam angular discrimination and energy resolution. Systematic TCS measurements are essential in studies of how the structure of target compound affects the electron-molecule interactions. They are also very useful in semi-empirical formula derivations. Such formula, in which the TCS value at given energy is related to some physico–chemical properties of the target molecule, can be utilized in predictions of the scattering intensity for molecular targets experimentally or theoretically not examined as yet. Analytical expression for the TCS dependence on the impact energy can be also useful in modeling applications.

This work has been supported in part by the Polish Ministry of Science and Higher Education (MNiSzW Project 2019–2020).

Author contribution statement

CzSz proposed the idea of presentation and contributed mainly to the text, while PM prepared the introduction and the graphical data presentation. Both authors were involved in the bibliographic studies, generation of the final manuscript version, and the answer to the referees' reports.

References

1. J.J. Thomson, Philos. Mag. **44**, 293 (1897)
2. P. Lenard, Ann. Phys. Lpz. **12**, 714 (1903)
3. J. Franck, G. Hertz, Verh. Dtsch. Phys. Ges. **16**, 457 (1914)
4. C. Ramsauer, Ann. Phys. Lpz. **64**, 513 (1921)
5. G.J. Schulz, Rev. Mod. Phys. **45**, 423 (1973)
6. K. Altwegg, H. Balsiger, A. Bar-Nun, J.-J. Bertheller, A. Bieler, P. Bochsler, C. Briois, U. Calmonte, M.R. Combi, H. Cottin, J. De Keyser, F. Dhooghe, B. Fiethe, S.A. Fuselier, S. Gase, T.I. Gombosi, K.C. Hansen, M. Haessig, A. Jäckel, E. Kopp, A. Korth, L. Le Roy, U. Mall, B. Marty, O. Mousis, T. Owen, H. Réme, M. Rubin, T. Sémon, C-Y. Tzou, J.H. Waiter, P. Wurz, Sci. Adv. **2**, e1600285 (2016)
7. S. Gasc, K. Altwegg, B. Fiethe, A. Jäckel, A. Korth, L. Le Roy, U. Mall, H. Réme, M. Rubin, J. Hunter Waite, P. Wurz, Planet. Space Sci. **135**, 64 (2017)
8. H. Rothard, A. Domaracka, P. Boduch, M.E. Palumbo, G. Strazulla, E.F. da Silveira, E. Dartois, J. Phys. B **50**, 062001 (2017)
9. K.E. Shulenberger, J.L. Zhu, K. Tran, S. Abdullahi, C. Belvin, J. Lukens, Z. Peeler, E. Mullikin, H.M. Cumberbatch, J. Huang, K. Regovich, A. Zhou, L. Heller, M. Markovic, L. Gates, C. Buffo, R. Tano-Menka, C.R. Arumainayagam, E. Böhle, P. Swiderek, S. Esmaili, A.D. Bass, M. Huels, L. Sanche, ACS Earth Space Chem. **3**, 800 (2019)
10. A. Lafosse, M. Bertin, A. Domaracka, D. Pliszka, E. Illenberger, R. Azria, Phys. Chem. Chem. Phys. **8**, 5564 (2006)
11. S. Esmaili, A.D. Bass, P. Cloutier, L. Sanche, M.A. Huels, J. Chem. Phys. **148**, 164702 (2018)
12. L. Sanche, J. Phys. B **23**, 1597 (1990)
13. B. Boudaiffa, P. Cloutier, D. Hunting, M.A. Huels, L. Sanche, Science **287**, 1658 (2000)
14. L. Sanche, Nature **461**, 358 (2009)
15. A.D. McKee, M.J. Schaible, R.A. Rosenberg, S. Kundu, T.M. Orlando, J. Chem. Phys. **150**, 204709 (2019)
16. L. Sanche, Eur. Phys. J. D **35**, 367 (2005)
17. J.D. Gornfinkiel, S. Ptasińska, J. Phys. B **50**, 182001 (2017)
18. V. Lemelin, L. Sanche, High-resolution electron energy loss spectroscopy: absolute cross section measurements for low energy electron scattering from biomolecules, in *Radiation in Bioanalysis: Spectroscopic Techniques and Theoretical Methods*, edited by A.S. Pereira, P. Tavares, P. Limão-Vieira (Springer International Publishing, 2019), pp. 3–42
19. M. Fuss, A. Muñoz, J.C. Oller, F. Blanco, P. Limão-Vieira, C. Huerga, M. Tellez, M.J. Hubin-Franskin, K. Nixon, M. Brunger, G. Garcia, J. Phys.: Conf. Ser. **194**, 012028 (2009)
20. H. Nikjoo, D. Emfietzglou, T. Liamsuwan, R. Taleei, D. Liljequist, S. Uehara, Rep. Prog. Phys. **79**, 116601 (2016)
21. M.J. Brunger, Int. Rev. Phys. Chem. **36**, 333 (2017)
22. M. Michaud, A. Wen, L. Sanche, Radiat. Res. **159**, 3 (2003)
23. Y. Itikawa, N. Mason, J. Phys. Chem. Ref. Data **34**, 1 (2001)
24. Cz. Szmytkowski, P. Możejko, Opt. Appl. **36**, 543 (2006)
25. G. Franz, *Low Pressure Plasmas and Microstructuring Technology* (Springer, Berlin, Heidelberg, 2009)
26. Z.L. Petrović, S. Dujko, D. Marić, G. Malović, Z. Nikitović, O. Sasić, J. Jovanović, V. Stojanović, M. Radmilović-Radenović, J. Phys. D. **42**, 194002 (2009)

27. L. Campbell, M.J. Brunger, Plasma Sources Sci. Technol. **22**, 013002 (2013)
28. L. Campbell, M.J. Brunger, Int. Rev. Phys. Chem. **35**, 297 (2016)
29. C.R. Arumainayagam, M.C. Boyer, K.E. Atkinson, The role of low-energy (<20 eV) electrons in atmospheric processes, in *Low-Energy Electrons: Fundamentals and Applications*, edited by O. Ingólfsson (Pan Stanford Publishing, Singapore, 2019), pp. 341–363
30. M. Huth, F. Porrati, O.V. Dobrovolskiy, Microelectron. Eng. **185–186**, 9 (2018)
31. D.H. Faibrother, S.G. Rosenberg, C.W. Hagen, I. Utke, P. Swiderek, Focused electron beam-induced processing, in *Low-Energy Electrons: Fundamentals and Applications*, edited by O. Ingólfsson (Pan Stanford Publishing, Singapore, 2019), pp. 219–270
32. S. Schippers, E. Sokell, F, Aumayr, H. Sadeghpour, K. Ueda, I. Bray, K. Bartschat, A. Murray, J. Tennyson, A. Dorn, M. Yamazaki, M. Takahashi, N. Mason, O. Novotny, A. Wolf, L. Sanche, M. Centurion, Y. Yamazaki, G. Laricchia, C.M. Surko, J. Sullivan, G. Gribakin, D.W. Savin, Y. Ralchenko, R. Hoekstra, G. O'Sullivan, J. Phys. B **52**, 171002 (2019)
33. R.B. Brode, Rev. Mod. Phys. **5**, 257 (1933)
34. J.H. McMillen, Rev. Mod. Phys. **11**, 84 (1939)
35. B. Bederson, L.J. Kieffer, Rev. Mod. Phys. **43**, 601 (1971)
36. B.H. Bransden, M.R.C. McDowell, Phys. Rep. **46**, 249 (1978)
37. Y. Itikawa, Phys. Rep. **46**, 117 (1978)
38. N.F. Lane, Rev. Mod. Phys. **52**, 29 (1980)
39. S. Trajmar, D.F. Register, A. Chutijan, Phys. Rep. **97**, 219 (1983)
40. A. Zecca, G.P. Karwasz, R.S. Brusa, La Rivista del Nuovo Cimento **19**, 1 (1996)
41. G.P. Karwasz, A. Zecca, R.S. Brusa, La Rivista del Nuovo Cimento **24(1)**, 1 (2001)
42. G.P. Karwasz, A. Zecca, R.S. Brusa, La Rivista del Nuovo Cimento **24(4)**, 1 (2001)
43. M.J. Brunger, S.J. Buckman, Phys. Rep. **357**, 215 (2002)
44. Y. Itikawa, editor, in *Photon and Electron Interactions with Atoms, Molecules and Ions* (Landoldt-Börnstein) (Springer, Berlin, 2000–2003), Vol. 17A–C
45. L.G. Christophorou, J.K. Olthoff, *Fundamental Electron Interactions with Plasma Processing Gases* (Kluwer Academic/Plenum Publishers, New York, 2004)
46. K. Anzai, H. Kato, M. Hoshino, Y. Itikawa, L. Campbell, M.J. Brunger, S.J. Buckman, H. Cho, F. Blanco. G. Garcia, P. Limão-Vieira, O. Ingólfsson, Eur. Phys. J. D **66**, 36 (2012)
47. R.E. Kennerly, R.A. Bonham, Phys. Rev. A **17**, 1844 (1978)
48. S. Trajmar, D.F. Register, Experimental techniques for cross-section measurements, in *Electron Molecule Collisions*, edited by I. Shimamura, K. Takayanagi (Plenum Press, New York, 1984), pp. 427–486
49. C. Ma, P.B. Lieschesk, R.A. Bonham, Rev. Sci. Instrum. **60**, 3661 (1989)
50. M.J. Brunger, Molecular processes and techniques for measuring their scattering cross sections, in *Low-Energy Electrons: Fundamentals and Applications*, edited by O. Ingólfsson (Pan Stanford Publishing, Singapore, 2019), pp. 1–36
51. S.P. Khare, *Introduction to the Theory of Collisions of Electrons with Atoms and Molecules* (Springer, New York, 2001)
52. H. Tanaka, M.J. Brunger, L. Campbell, H. Kato, M. Hoshino, A.R.P. Rau, Rev. Mod. Phys. **88**, 025004 (2016)
53. K.N. Joshipura, N. Mason, *Atomic-Molecular Ionization by Electron Scattering* (Cambridge University Press, 2019)
54. G.G. Raju, *Gaseous Electronics: Tables, Atoms and Molecules* (CRC Press, 2012)
55. G.P. Karwasz, A. Zecca, R.S. Brusa, Chapter VI.1. Electron scattering with molecules. Total scattering cross sections, in *Photon and Electron Interaction, with Atoms, Molecules and Ions, Landolt-Börstein New Series* (Springer-Verlag, Berlin, Heidelberg, 2003), Vol. I/17 C
56. H. Kato, S. Kobayashi, C. Makochekanwa, M. Hoshino, N. Shinohara, O. Sueoka, H. Cho, H. Tanaka, Phys. Rev. A **79**, 062702 (2009)
57. R.N. Nelson, S.O. Colgate, Phys. Rev. A **8**, 3045 (1973)
58. J.P. Sullivan, C. Makochekanwa, A. Jones, P. Caradonna, D.S. Slaughter, J. Machacek, R.P. McEachran, D.W. Mueller, S.J. Buckman, J. Phys. B **44**, 035201 (2011)
59. M. Knudsen, Ann. Phys. Lpz. **31**, 205 (1910)
60. K.F. Poulter, M.J. Rodgers, P.J. Nash, T.J. Thompson, M.P. Perkin, Vacuum **33**, 311 (1983)
61. B. Daudé, H. Elandaloussi, C. Jansen, Vacuum **104**, 77 (2014)
62. M. Kitajima, T. Kishino, T. Okumura, N. Kobayashi, A. Sayama, Y. Mori, K. Hosaka, T. Odagiri, M. Hoshino, H. Tanaka, Eur. Phys. J. D **71**, 139 (2017)
63. A.I. Lozano, J.C. Oller, K. Krupa, F. Ferreira da Silva, P. Limão-Vieira, F. Blanco, A. Muñoz, R. Colmenares, G. Garcia, Rev. Sci. Instrum. **89**, 063105 (2018)
64. R.E. Kennerly, Phys. Rev. A **21**, 1876 (1980)
65. G. Dalba, P. Fornasini, R. Grisenti, G. Ranieri, A. Zecca, J. Phys. B **13**, 4695 (1980)
66. K.R. Hoffman, M.S. Dababneh, Y.F. Hsieh, W.E. Kauppila, V. Pol, J.H. Smart, T.S. Stein, Phys. Rev. A **25**, 1393 (1982)
67. H. Nishimura, K. Yano, J. Phys. Soc. Jpn. **57**, 1951 (1988)
68. W. Sun, M.A. Morrison, W.A. Isaacs, W.K. Trail, D.T. Alle, R.J. Gulley, M.J. Brennan, S.J. Buckman, Phys. Rev. A **52**, 1229 (1995)
69. Cz. Szmytkowski, K. Maciąg, G. Karwasz, Phys. Scr. **54**, 271 (1996)
70. S.V. Hoffmann, S.L. Lunt, N.C. Jones, D. Field, J.-P. Ziesel, Rev. Sci. Instrum. **73**, 4157 (2002)
71. T. Okumura, N. Kobayashi, A. Sayama, Y. Mori, H. Akasaka, K. Hosaka, T. Odagiri, M. Hoshino, M. Kitajima, J. Phys. B **52**, 035201 (2019)
72. G. Sunshine, B.B. Aubrey, B. Bederson, Phys. Rev. **154**, 1 (1967)
73. A. Salop, H.H. Nakano, Phys. Rev. A **2**, 127 (1970)
74. Y. Katayama, S. Mori, O. Sueoka, At. Coll. Res. Jpn. Prog. Rep. **11**, 22 (1985)
75. M.S. Dababneh, Y.-F. Hsieh, W.E. Kauppila, C.K. Kwan, S.J. Smith, T.S. Stein, M.N. Uddin, Phys. Rev. A **38**, 1207 (1988)
76. K.P. Subramanian, V.J. Kumar, J. Phys. B **23**, 745 (1990)
77. I. Kanik, J.C. Nickel, S.J. Trajmar, J. Phys. B **25**, 2189 (1992)

78. S.J. Buckman, D.T. Alle, M.J. Brennan, P.B. Burrow, J.C. Gibson, R.J. Gulley, M. Jacka, D.S. Newman, A.R.P. Rau, J.P. Sullivan, K.W. Trantham, Aust. J. Phys. **52**, 473 (1999)
79. R. Kadokura, A. Loreti, Á. Kövér, A. Faure, J. Tennyson, G. Laricchia, Phys. Rev. Lett. **123**, 033401 (2019)
80. O. Sueoka, S. Mori, Y. Katayama, J. Phys. B **19**, L373 (1986)
81. A. Zecca, G.P. Karwasz, S. Oss, R. Grisenti, R.S. Brusa, J. Phys. B **20**, L133 (1987)
82. Cz. Szmytkowski, Chem. Phys. Lett. **13**, 363 (1987)
83. Z. Sağlam, N. Aktekin, J. Phys. B **23**, 1529 (1990)
84. Z. Sağlam, N. Aktekin, J. Phys. B **24**, 3491 (1991)
85. M. Kimura, O. Sueoka, A. Hamada, Y. Itikawa, Adv. Chem. Phys. **111**, 537 (2000)
86. P. Możejko, A. Domaracka, M. Zawadzki, E. Ptasińska-Denga, Cz. Szmytkowski, J. Phys. Conf. Ser. **875**, 062047 (2017)
87. Cz. Szmytkowski, P. Możejko, E. Ptasińska-Denga, A. Sabisz, Phys. Rev. A **82**, 032701 (2010)
88. A.I. Lozano, A. Loupas, F. Blanco, J.D. Gorfinkiel, G. Garcia, J. Chem. Phys. **149**, 134303 (2018)
89. A. Traoré Dubuis, A. Verkhovtsev, L. Ellis-Gibbings, K. Krupa, F. Blanco, D.B. Jones, M.J. Brunger, G. Garcia, J. Chem. Phys. **147**, 054301 (2017)
90. P. Możejko, E. Ptasińska-Denga, Cz. Szmytkowski, Eur. Phys. J. D **66**, 44 (2012)
91. W.Y. Baek, M. Bug, H. Rabus, E. Gargioni, B. Grosswendt, Phys. Rev. A **86**, 032702 (2012)
92. A. Zecca, C. Perazzolli, M.J. Brunger, J. Phys. B: At. Mol. Opt. Phys. **38**, 2079 (2005)
93. P. Możejko, E. Ptasińska-Denga, A. Domaracka, Cz. Szmytkowski, Phys. Rev. A **74**, 012708 (2006)
94. M. Fuss, A. Muñoz, J.C. Oller, F. Blanco, D. Almeida, P. Limão-Vieira, T.P.D. Do, M.J. Brunger, G. Garcia, Phys. Rev. A **80**, 052709 (2009)
95. N.A. Garland, M.J. Brunger, G. Garcia, J. de Urquijo, R.D. White, Phys. Rev. A **88**, 062712 (2013)
96. P. Możejko, A. Domaracka, E. Ptasińska-Denga, Cz. Szmytkowski, Chem. Phys. Lett. **429**, 378 (2006)
97. I.V. Chernyshova, E.E. Kontrosh, P.P. Markush, O.B. Shpenik, Tech. Phys. Lett. **43**, 998 (2017)
98. F. Costa, L. Álvarez, A.I. Lozano, F. Blanco, J.C. Oller, A. Muñoz, A. Souza Barbosa, M.H.F. Bettega, F. Ferreira da Silva, P. Limão-Vieira, R.D. White, M.J. Brunger, G. Garcia, J. Chem. Phys. **151**, 084310 (2019)
99. W. Holst, J. Holtsmark, K. Nor, Vidensk. Selsk. **4**, 89 (1931)
100. P. Możejko, G. Kasperski, Cz. Szmytkowski, G.P. Karwasz, R.S. Brusa, A. Zecca, Chem. Phys. Lett. **257**, 309 (1996)
101. R.J. Gulley, S.L. Lunt, J.-P. Ziesel, D. Field, J. Phys. B **31**, 2735 (1998)
102. C. Makochekanwa, O. Sueoka, M. Kimura, Phys. Rev. A **68**, 032707 (2003)
103. R.F. da Costa, E.M. de Oliveira, M.H.F. Bettega, M.T.N. Varella, D.B. Jones, M.J. Brunger, F. Blanco, R. Colmenares, P. Limão-Vieira, G. Garcia, M.A.P. Lima, J. Chem. Phys. **142**, 104304 (2015)
104. H. Kato, C. Makochekanwa, Y. Shiroyama, M. Hoshino, N. Shinohara, O. Sueoka, M. Kimura, H. Tanaka, Phys. Rev. A **75**, 062705 (2007)
105. A. Traoré Dubuis, F. Costa, F. Ferreira da Silva, P. Limão-Vieira, J.C. Oller, F. Blanco, G. Garcia, Chem. Phys. Lett. **699**, 182 (2018)
106. A.I. Lozano, J. Jiménez, F. Blanco, G. Garcia, Phys. Rev. A **98**, 012709 (2018)
107. Cz. Szmytkowski, S. Stefanowska, N. Tańska, B. Żywicka, E. Ptasińska-Denga, P. Możejko, Mol. Phys. **117**, 395 (2019)
108. W.Y. Baek, A. Arndt, M.U. Bug, H. Rabus, M. Wang, Phys. Rev. A **88**, 032702 (2013)
109. M.C. Fuss, A.G. Sanz, F. Blanco, J.C. Oller, P. Limão-Vieira, M.J. Brunger, G. Garcia, Phys. Rev. A **88**, 042702 (2013)
110. A.G. Sanz, M.C. Fuss, F. Blanco, J.D. Gorfinkiel, D. Almeida, F. Ferreira da Silva, P. Limão-Vieira, M.J. Brunger, G. Garcia, J. Chem. Phys. **139**, 184310 (2013)
111. Cz. Szmytkowski, E. Ptasińska-Denga, J. Phys. B **44**, 015203 (2011)
112. A.I. Lozano, J.C. Oller, D.B. Jones, R.F. da Costa, M.T.N. Varella, M.H.F. Bettega, F. Ferreira da Silva, P. Limão-Vieira, M.A.P. Lima, R.D. White, M.J. Brunger, F. Blanco, A. Muñoz, G. Garcia, Phys. Chem. Chem. Phys. **20**, 22368 (2018)
113. A.I. Lozano, F. Ferreira da Silva, F. Blanco, P. Limão-Vieira, G. Garcia, Chem. Phys. Lett. **706**, 533 (2018)
114. Cz. Szmytkowski, M. Piotrowicz, A. Domaracka, Ł. Kłosowski, E. Ptasińska-Denga, G. Kasperski, J. Chem. Phys. **121**, 1790 (2004)
115. Cz. Szmytkowski, A. Domaracka, P. Możejko, E. Ptasińska-Denga, Ł. Kłosowski, M. Piotrowicz, G. Kasperski, Phys. Rev. A **70**, 032707 (2004)
116. Cz. Szmytkowski, J. Phys. B **43**, 055201 (2010)
117. Cz. Szmytkowski, P. Możejko, E. Ptasińska-Denga, J. Phys. B **44**, 205202 (2011)
118. D.G.M. Silva, T. Tejo, J. Muse, D. Romero, M.A. Khakoo, M.C.A Lopes, J. Phys. B **43**, 015201 (2010)
119. D.G.M. da Silva, M. Gomes, S. Ghosh, I.F.L. Silva, W.A.D. Pires, D.B. Jones, F. Blanco, G. Garcia, S.J. Buckman, M.J. Brunger, M.C.A. Lopes, J. Chem. Phys. **147**, 194307 (2017)
120. M. Gomes, D.G.M. da Silva, A.C.P. Fernandes, S. Ghosh, W.A.D. Pires, D.B. Jones, F. Blanco, G. Garcia, M.J. Brunger, M.C.A. Lopes, J. Chem. Phys. **150**, 194307 (2019)
121. F. Schmieder, Z. Elektrochem. **36**, 700 (1930)
122. O. Sueoka, Y. Katayama, S. Mori, At. Coll. Res. Jpn. Prog. Rep. **11**, 17 (1985)
123. Cz. Szmytkowski, A. Krzysztofowicz, J. Phys. B **28**, 4291 (1995)
124. A.I. Lozano, L. Álvarez, F. Blanco, M.J. Brunger, G. Garcia, J. Chem. Phys. **149**, 244304 (2018)
125. A. Krzysztofowicz, Cz. Szmytkowski, J. Phys. B **28**, 1593 (1995)
126. S. Stefanowska-Tur, P. Możejko, E. Ptasińska-Denga, Cz. Szmytkowski, J. Chem. Phys. **150**, 094303 (2019)
127. P. Możejko, S. Stefanowska-Tur, E. Ptasińska-Denga, Cz. Szmytkowski, J. Chem. Phys. **151**, 064305 (2019)
128. A. Zecca, G.P. Karwasz, R.S. Brusa, Cz. Szmytkowski, J. Phys. B **24**, 2747 (1991)
129. Cz. Szmytkowski, P. Możejko, G. Kasperski, J. Phys. B **30**, 4363 (1997)
130. P. Możejko, G. Kasperski, Cz. Szmytkowski, J. Phys. B **29**, L571 (1996)

131. Cz. Szmytkowski, P. Możejko, G. Kasperski, J. Phys. B **31**, 3917 (1998)
132. Cz. Szmytkowski, A.M. Krzysztofowicz, P. Janicki, L. Rosenthal, Chem. Phys. Lett. **199**, 191 (1992)
133. P. Możejko, G. Kasperski, Cz. Szmytkowski, A. Zecca, G.P. Karwasz, L. Del Longo, R.S. Brusa, Eur. Phys. J. D **6**, 481 (1999)
134. Cz. Szmytkowski, S. Kwitnewski, J. Phys. B **35**, 2613 (2002)
135. Cz. Szmytkowski, S. Kwitnewski, E. Ptasińska-Denga, Phys. Rev. A **68**, 032715 (2003)
136. P. Możejko, E. Ptasińska-Denga, Cz. Szmytkowski, M. Zawadzki, J. Phys. B **45**, 145203 (2012)
137. Cz. Szmytkowski, S. Stefanowska, M. Zawadzki, E. Ptasińska-Denga, P. Możejko, J. Chem. Phys. **143**, 064306 (2015)
138. Cz. Szmytkowski, P. Możejko, M. Zawadzki, E. Ptasińska-Denga, J. Phys. B **46**, 065203 (2013)
139. Cz. Szmytkowski, P. Możejko, M. Zawadzki, K. Maciąg, E. Ptasińska-Denga, Phys. Rev. A **89**, 052702 (2014)
140. Cz. Szmytkowski, S. Kwitnewski, J. Phys. B **35**, 3781 (2002)
141. Cz. Szmytkowski, P. Możejko, M. Zawadzki, E. Ptasińska-Denga, J. Phys. B **48**, 025201 (2015)
142. Cz. Szmytkowski, S. Stefanowska, E. Ptasińska-Denga, P. Możejko, J. Electron Spectrosc. Relat. Phenom. **222**, 24 (2018)
143. Cz. Szmytkowski, S. Stefanowska, M. Zawadzki, E. Ptasińska-Denga, P. Możejko, Phys. Rev. A **94**, 042706 (2016)
144. P. Wickramarachchi, P. Palihawadana, G. Villela, W.M. Ariyasinghe, Nucl. Instrum. Methods B **267**, 3391 (2009)
145. W.M. Ariyasinghe, G. Vilela, Nucl. Instrum. Methods B **268**, 2217 (2010)
146. C. Makochekanwa, H. Kawate, O. Sueoka, M. Kimura, M. Kitajima, M. Hoshino, H. Tanaka, Chem. Phys. Lett. **368**, 82 (2003)
147. S.L. Xing, Q.C. Shi, X.J. Chen, K.Z. Xu, B.X. Yang, S.L. Wu, R.F. Feng, Phys. Rev. A **51**, 414 (1995)